International Journal of Multidisciplinary Trends

E-ISSN: 2709-9369
P-ISSN: 2709-9350
Impact Factor (RJIF): 6.32
www.multisubjectjournal.com
IJMT 2025; 7(11): 196-218
Received: 21-08-2025
Accepted: 25-09-2025

Se-Hun Jong
Faculty of Mechanical Science and Technology, Kim Cheak University of Technology, Kyogudong No.60, Yonggwang Street, Pyongyang, Democratic People's Republic of Korea

Hyon-Guk Jo
Faculty of Mechanical Science and Technology, Kim Cheak University of Technology, Kyogudong No.60, Yonggwang Street, Pyongyang, Democratic People's Republic of Korea

Kum-Song Ri
Faculty of Mechanical Science and Technology, Kim Cheak University of Technology, Kyogudong No.60, Yonggwang Street, Pyongyang, Democratic People's Republic of Korea

Corresponding Author:
Se-Hun Jong
Faculty of Mechanical Science and Technology, Kim Cheak University of Technology, Kyogudong No.60, Yonggwang Street, Pyongyang, Democratic People's Republic of Korea

Free vibration and stationary stochastic response analyses of heated composite laminated plate with varying thickness and curvilinear fiber using a meshfree method

Se-Hun Jong, Hyon-Guk Jo and Kum-Song Ri

DOI: https://www.doi.org/10.22271/multi.2025.v7.i11c.849

Abstract
In this paper, a meshfree Jacobi point interpolation (MJPI) approach for the free vibration and stationary stochastic response analyses of heated composite laminated plate with varying thickness and curvilinear fiber is developed. The theoretical formulations for heated composite laminated plate with varying thickness and curvilinear fiber are established by using Hamilton's principle in framework of first order shear deformation theory (FSDT). The effect of thermal stress generated by the temperature variation are considered based on the thermo-elastic theory. The displacement components of the plate are approximated by using the MJPI shape function. The boundary conditions considered in this study are achieved by using the artificial spring technique. The accuracy and reliability of the proposed MJPI shape function are confirmed by comparing with numerical results from the published literature and finite element software ABAQUS. Finally, the effects of different parameters such as temperature difference, fiber direction coefficient, thickness gradient and thickness power index on the free vibration and stationary stochastic response of the composite laminated plate are investigated.

Keywords: Meshfree Jacobi point interpolation, free vibration, stochastic response, varying thickness, curvilinear fiber

Introduction
Recently, the application fields of composite laminated plates and shells has been rapidly expanding to various engineering such as mechanical, civil, aerospace, marine, automotive, etc., due to their remarkable characteristics [1]. Therefore, the numerical and experimental studies of the dynamic behavior for composite plates and shells have been received considerable attention of many scholars [2-4]. Qin *et al.* [5] presented a Jacobi-Ritz method for the free vibration analysis of composite laminated plates subject to general boundary conditions. The displacement components of the plate were expanded by using Jacobi polynomials, and the Ritz method was used for the solution procedure on the basis of the energy functions. Zhang *et al.* [6] expanded the displacement components of the moderately thick laminated composite rectangular plate with different non-uniform boundary conditions by using two-dimensional Fourier series composed of the standard cosine series and the standard sine series. Wang *et al.* [7] dealt with the dynamics and power flow control of the irregular elastic coupled plate system including the quadrilateral/quadrilateral coupled system, the quadrilateral/triangle coupled system and the triangle/triangle coupled system. By using improved Fourier series method, Zhao *et al.* [8] investigated the free vibration behavior of functionally graded porous rectangular plate, in which the uniform or non-uniform distributions of porosity was assumed along a certain direction. Javani *et al.* [9] investigated the free vibration behavior of T-shape laminated composite plates reinforced with the graphene platelets by using the generalized differential quadrature element method.
In order to study the static and dynamic behaviors of the plates and shells, various theories including classical plate theory (CPT) [10, 11], FSDT [5, 12], high order shear deformation theory (HSDT) [13-15] and three-dimensional theory [16-18] are employed. Two-dimensional theories are based on the Kirchhoff hypothesis that normals to the middle surface remain normal to the deformed middle surface and suffer no extension [19].

Among the two-dimensional theories, FSDT is widely used for dynamic analysis of different shells and plates because of its high accuracy and low computational cost [20]. In framework of FSDT, Ye *et al.* [21] performed the free vibration analysis of moderately thick composite laminated plates with general boundary restraints and internal line supports by using a modified Fourier solution method. Li *et al.* [22] analyzed the vibration characteristic of functionally graded (FG) structures with general edge restraints on basis of multi-segment partitioning strategy and FSDT. In their study, the displacement functions are expanded by the Jacobi polynomials along the axial direction and Fourier series along the circumferential direction.

In general, the main applications of composite plates and shells are in high temperature situation, and mechanical properties of the composite structures are changed significantly in the thermal environment [23, 24]. Therefore, many scholars investigated the effect of thermal load on the free vibrations and dynamic responses of composite structures [25-28]. Soureshjani *et al.* [29] investigated the effects of temperature on free vibration of carbon nanotube reinforced composite joined conical-conical shells with temperature-dependent material. The static and dynamic behavior of the exponential functionally graded piezoelectric material plate subjected to the thermo-electric-mechanical loading were investigated by Kumar and Harsha [30], in which the governing equation considered the piezoelectric coupling effect and the geometric nonlinearity was derived by employing Hamilton's principle. Kumar *et al.* [31] investigated the free vibration behavior of FG doubly curved shallow stiffened shells with simply supported at all edges in the thermal environment. Rout *et al.* [32] performed the free vibration analyses of graphene reinforced singly and doubly curved laminated composite shell panels subjected to thermal load by means of finite element method (FEM) in framework of HSDT, in which the distortion of the geometry due to thermal loading was expressed by using the nonlinear part of Green-Lagrange strain.

The composite plates and shells with varying thickness are widely used in different industrial fields due to the advantages of their low weights and small dimensions. In the recent years, several studies on the dynamic characteristics of the composite plates and shells with varying thickness were performed [33-35]. Taati *et al.* [36] investigated the free vibration behavior of thin cylindrical shells rotating with a constant angular velocity based on the classical Donnell's and Love's shell theories, in which the axisymmetric variation of thickness was considered. The vibration characteristics of rotating functionally graded circular cylindrical shells with the linearly varying thickness along the longitudinal direction were studied by Quoc *et al.* [37]. The vibration characteristics of the laminated shells with curvilinear fiber were investigated by Nie [38] and Kwak [39].

A common type of the external load is random excitation such as the earthquakes, winds and jet noise, therefore, it is important to study the stochastic response of the composite plate and shell [40-42]. Zhou *et al.* [43] presented the theoretical formulation for the stationary/nonstationary stochastic response analyses of the heated composite laminated plate excited by different type of random excitations including concentrated excitation, distributed excitation and base acceleration excitation. In their study, the effect of some parameters including boundary condition, temperature variation on the power spectral density (PSD) functions of displacement and acceleration responses was investigated. Chen *et al.* [44] derived the analytical PSD functions of the stationary random responses for thin plate under base acceleration excitation based on pseudo excitation method (PEM). Yang *et al.* [45] determined the fully nonstationary random responses of rectangular Kirchhoff plates excited by temporally and spectrally nonstationary acceleration by using the discrete analytical method (DAM).

This study describes a MJPI formulation for the free vibration and stationary stochastic response analyses of heated composite laminated plate with varying thickness and curvilinear fiber. The Hamilton's principle is adopted to derive the governing equations and boundary conditions of the heated composite plate, in which the effect of varying thickness and curvilinear fiber on the stiffness of the plate is considered. The MJPI shape function using the Jacobi polynomials as the basis is presented to employ for approximate the displacement components of the heated plate structures. The thermal strains induced by the temperature difference are obtained from the nonlinear part of the Green-Lagrange strain. Some numerical examples show the good convergence, accuracy and reliability of the proposed method. Finally, effects of temperature difference, fiber direction coefficient, thickness gradient and power index on the vibrational behavior and stationary stochastic response of laminated plate are presented.

Theoretical formulations

In this section, the governing equations of the heater composite laminated plate with varying thickness and curvilinear fiber are derived by using Hamilton's principle in framework of FSDT. And the two-dimensional MJPI shape function using Jacobi polynomials as basis is presented. Then, the displacement components of the plate are approximated by the MJPI shape function.

Description of the model

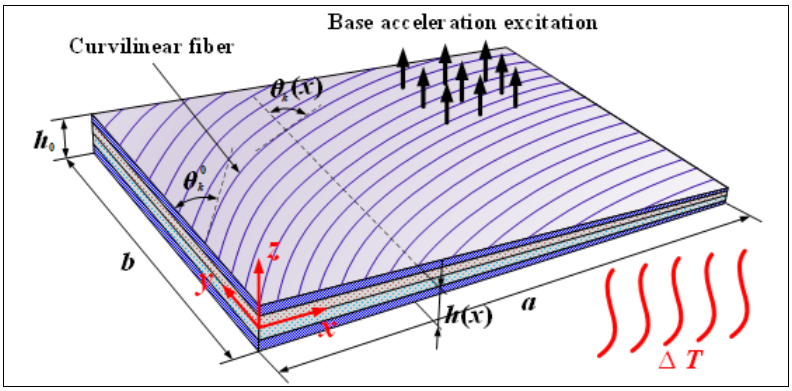

Fig 1: Geometry of heated composite laminated plate with varying thickness and curvilinear fiber.

In this paper, a composite laminated plate with varying thickness and curvilinear fiber in thermal environment is considered, as shown in Fig.1. The composite plate with length a and width b is affected by temperature difference ΔT and stationary base acceleration excitation.
As shown in Fig. 1, an orthogonal coordinate system (x, y, z) is introduced into the middle surface of the plate. The thickness of the composite laminated plate under consideration is expressed as a function of x-coordinate.

$$h(x) = h_0\left[1-\eta\left(x/a\right)^p\right] \tag{1}$$

where h_0, η and p indicates the initial thickness of the plate, the thickness gradient and the thickness power index in x direction, respectively.
Besides, the fiber angle in kth layer of the composite laminated plate is expressed as

$$\theta_k(x) = \theta_k^0 + \lambda x$$

where λ and θ_k^0 denote the fiber direction coefficient and the initial fiber angle of kth layer.

Governing equations of heated composite laminated plate with varying thickness and curvilinear fiber
By the assumption of FSDT, the displacement components of a moderately thick plate in the x, y and z directions are expressed as the following linear relationships.

$$\begin{cases} U(x,y,z,t) = u(x,y,t) + z\psi_x(x,y,t) \\ V(x,y,z,t) = v(x,y,t) + z\psi_y(x,y,t) \\ W(x,y,z,t) = w(x,y,t) \end{cases} \tag{3}$$

where u, v and w represent the displacement components on the middle surface of considered plate in the x, y and z directions, and ψ_x, ψ_y are the rotations of transverse normal respect to y and x axes, respectively.
In the middle surface of composite laminated plate, the matrix form of displacement-strain relationships can be expressed as

$$\boldsymbol{\varepsilon} = \boldsymbol{B}\boldsymbol{u} \tag{4}$$

where $\boldsymbol{\varepsilon}$, $\boldsymbol{u}$ and $\boldsymbol{B}$ represent the strain, displacement vectors and the partial differential operator matrix, respectively.
The strain vector $\boldsymbol{\varepsilon}$ is composed of the middle surface strains and the curvature changes as

$$\boldsymbol{\varepsilon} = \left[\varepsilon_x^0 \quad \varepsilon_y^0 \quad \gamma_{xy}^0 \quad \chi_x \quad \chi_y \quad \chi_{xy} \quad \gamma_{yz}^0 \quad \gamma_{xz}^0\right]^T \tag{5}$$

where ε_i^0, γ_{ij}^0, χ_i and χ_{ij} (i, j=x, y) represent the normal strain, shear strain, curvature change and twist change, respectively.
The displacement vector $\boldsymbol{u}$ is composed of the middle surface displacements as

$$\boldsymbol{u} = \left[u \quad v \quad w \quad \psi_x \quad \psi_y\right]^T \tag{6}$$

The partial differential operator matrix $\boldsymbol{B}$ is expressed as

$$\boldsymbol{B} = \begin{bmatrix} \partial/\partial x & 0 & \partial/\partial y & 0 & 0 & 0 & 0 & 0 \\ 0 & \partial/\partial y & \partial/\partial x & 0 & 0 & 0 & 0 & 0 \\ 0 & 0 & 0 & 0 & 0 & 0 & \partial/\partial y & \partial/\partial x \\ 0 & 0 & 0 & \partial/\partial x & 0 & \partial/\partial y & 0 & 1 \\ 0 & 0 & 0 & 0 & \partial/\partial y & \partial/\partial x & 1 & 0 \end{bmatrix}^T \tag{7}$$

The relationship between internal forces and strains are expressed as

$$\boldsymbol{N} = \boldsymbol{D}\boldsymbol{\varepsilon} \tag{8}$$

where the internal force vector $\boldsymbol{N}$ is as

$$\boldsymbol{N} = \left[N_x \quad N_y \quad N_{xy} \quad M_x \quad M_y \quad M_{xy} \quad Q_y \quad Q_x\right]^T \tag{9}$$

where N_i, N_{ij} and Q_i denote the normal, shear and transverse shear forces, respectively. M_i and M_{ij} are the bending and twisting moments.

The material property matrix $\boldsymbol{D}$ is expressed as

$$\boldsymbol{D}=\begin{bmatrix} A_{11} & A_{12} & A_{16} & B_{11} & B_{12} & B_{16} & 0 & 0 \\ A_{12} & A_{22} & A_{26} & B_{12} & B_{22} & B_{26} & 0 & 0 \\ A_{16} & A_{26} & A_{66} & B_{16} & B_{26} & B_{66} & 0 & 0 \\ B_{11} & B_{12} & B_{16} & D_{11} & D_{12} & D_{16} & 0 & 0 \\ B_{12} & B_{22} & B_{26} & D_{12} & D_{22} & D_{26} & 0 & 0 \\ B_{16} & B_{26} & B_{66} & D_{16} & D_{26} & D_{66} & 0 & 0 \\ 0 & 0 & 0 & 0 & 0 & 0 & A_{44} & A_{45} \\ 0 & 0 & 0 & 0 & 0 & 0 & A_{45} & A_{55} \end{bmatrix} \tag{10}$$

The components of the matrix $\boldsymbol{D}$ are as

$$A_{ij}=\begin{cases} \sum_{k=1}^{N_L} Q_{ij}^{k}\left(z_{k+1}-z_{k}\right) & i,j=1,2,6 \\ k_c\sum_{k=1}^{N_L} Q_{ij}^{k}\left(z_{k+1}-z_{k}\right) & i,j=4,5 \end{cases} \qquad B_{ij}=\frac{1}{2}\sum_{k=1}^{N_L} Q_{ij}^{k}\left(z_{k+1}^{2}-z_{k}^{2}\right) \quad i,j=1,2,6$$

$$D_{ij}=\frac{1}{3}\sum_{k=1}^{N_L} Q_{ij}^{k}\left(z_{k+1}^{3}-z_{k}^{3}\right) \quad i,j=1,2,6 \tag{11}$$

where N_L and k_c represent the number of layer and shear correction factor, which is selected as 5/6.
In the composite laminated plate with varying thickness, z-coordinate of kth layer can be expressed as

$$z_k(x)=h_0\left(\frac{k-1}{N_L}-0.5\right)\left[1-\eta\left(\frac{x}{a}\right)^{p}\right] \tag{12}$$

Substituting the above equation into Eq. (11)

$$A_{ij}=\begin{cases} \sum_{k=1}^{N_L}\frac{Q_{ij}^{k}h_0}{N_L}\left[1-\eta\left(\frac{x}{a}\right)^{p}\right], & i,j=1,2,6 \\ k_c\sum_{k=1}^{N_L}\frac{Q_{ij}^{k}h_0}{N_L}\left[1-\eta\left(\frac{x}{a}\right)^{p}\right], & i,j=4,5 \end{cases} \tag{13}$$

$$B_{ij}=\frac{1}{2}\sum_{k=1}^{N_L} Q_{ij}^{k}h_0^{2}\left[1-\eta\left(\frac{x}{a}\right)^{p}\right]^{2}\left[\left(\frac{k}{N_L}-0.5\right)^{2}-\left(\frac{k-1}{N_L}-0.5\right)^{2}\right], \quad i,j=1,2,6$$

$$D_{ij}=\frac{1}{3}\sum_{k=1}^{N_L} Q_{ij}^{k}h_0^{3}\left[1-\eta\left(\frac{x}{a}\right)^{p}\right]^{3}\left[\left(\frac{k}{N_L}-0.5\right)^{3}-\left(\frac{k-1}{N_L}-0.5\right)^{3}\right], \quad i,j=1,2,6$$

Considering Eq. (2), the elastic stiffness coefficients of the kth layer of composite laminated plate with curvilinear fiber can be written as

$$Q_{11}^{k}=Q_{11}\cos^{4}(\theta_k^{0}+\lambda x)+\frac{(Q_{12}+2Q_{66})}{2}\sin^{2}2(\theta_k^{0}+\lambda x)+Q_{22}\sin^{4}(\theta_k^{0}+\lambda x)$$

$$Q_{12}^{k}=\frac{(Q_{11}+Q_{22}-4Q_{66})}{4}\sin^{2}2(\theta_k^{0}+\lambda x)+Q_{12}\left[\sin^{4}(\theta_k^{0}+\lambda x)+\cos^{4}(\theta_k^{0}+\lambda x)\right]$$

$$Q_{16}^{k}=Q_{11}\sin(\theta_k^{0}+\lambda x)\cos^{3}(\theta_k^{0}+\lambda x)-Q_{22}\sin^{3}(\theta_k^{0}+\lambda x)\cos(\theta_k^{0}+\lambda x) -\frac{(Q_{12}+2Q_{66})}{4}\sin 4(\theta_k^{0}+\lambda x)$$

$$Q_{22}^{k}=Q_{11}\sin^{4}(\theta_k^{0}+\lambda x)+Q_{22}\cos^{4}(\theta_k^{0}+\lambda x)+\frac{(Q_{12}+2Q_{66})}{2}\sin^{2}2(\theta_k^{0}+\lambda x) \tag{14}$$

$$Q_{26}^{k} = Q_{11}\sin^{3}(\theta_{k}^{0}+\lambda x)\cos(\theta_{k}^{0}+\lambda x) - Q_{22}\sin(\theta_{k}^{0}+\lambda x)\cos^{3}(\theta_{k}^{0}+\lambda x) + \frac{(Q_{12}+2Q_{66})}{4}\sin 4(\theta_{k}^{0}+\lambda x)$$

$$Q_{44}^{k} = Q_{44}\cos^{2}(\theta_{k}^{0}+\lambda x) + Q_{55}\sin^{2}(\theta_{k}^{0}+\lambda x)$$

$$Q_{45}^{k} = \frac{(Q_{55}-Q_{44})}{2}\sin 2(\theta_{k}^{0}+\lambda x)$$

$$Q_{55}^{k} = Q_{44}\sin^{2}(\theta_{k}^{0}+\lambda x) + Q_{55}\cos^{2}(\theta_{k}^{0}+\lambda x)$$

$$Q_{66}^{k} = \frac{(Q_{11}+Q_{22}-2Q_{12})}{4}\sin^{2} 2(\theta_{k}^{0}+\lambda x) + Q_{66}\cos^{2} 2(\theta_{k}^{0}+\lambda x)$$

where Q_{ij} indicates the reduced stiffness coefficient of the orthotropic material.

When the composite laminated plate is affected by thermal load ΔT, the thermal stresses of the kth layer of the plate are expressed as

$$\begin{Bmatrix} \sigma_{x}^{Tk} \\ \sigma_{y}^{Tk} \\ \tau_{xy}^{Tk} \end{Bmatrix} = -\begin{bmatrix} Q_{11}^{k} & Q_{12}^{k} & Q_{16}^{k} \\ Q_{12}^{k} & Q_{22}^{k} & Q_{26}^{k} \\ Q_{16}^{k} & Q_{26}^{k} & Q_{66}^{k} \end{bmatrix} \begin{Bmatrix} \alpha_{11}^{k}\Delta T \\ \alpha_{22}^{k}\Delta T \\ \alpha_{12}^{k}\Delta T \end{Bmatrix} \tag{15}$$

where α_{ij}^{k} is the thermal expansion coefficient expressed as

$$\begin{aligned} \alpha_{11}^{k} &= \alpha_{11}\cos^{2}(\theta_{k}^{0}+\lambda x) + \alpha_{22}\sin^{2}(\theta_{k}^{0}+\lambda x) - \alpha_{12}\sin(\theta_{k}^{0}+\lambda x)\cos(\theta_{k}^{0}+\lambda x) \\ \alpha_{22}^{k} &= \alpha_{11}\sin^{2}(\theta_{k}^{0}+\lambda x) + \alpha_{22}\cos^{2}(\theta_{k}^{0}+\lambda x) + \alpha_{12}\sin(\theta_{k}^{0}+\lambda x)\cos(\theta_{k}^{0}+\lambda x) \\ \alpha_{12}^{k} &= (\alpha_{11}-\alpha_{22})\sin 2(\theta_{k}^{0}+\lambda x) + \alpha_{12}\cos 2(\theta_{k}^{0}+\lambda x) \end{aligned} \tag{16}$$

where α_{ij} represent the linear thermal expansion coefficients.

The thermal strains induced by the temperature difference can be expressed by the nonlinear part of the Green-Lagrange strain.

$$\begin{aligned} \varepsilon_{x}^{NL} &= \left(\frac{\partial U}{\partial x}\right)^{2} + \left(\frac{\partial V}{\partial x}\right)^{2} + \left(\frac{\partial W}{\partial x}\right)^{2} \\ \varepsilon_{y}^{NL} &= \left(\frac{\partial U}{\partial y}\right)^{2} + \left(\frac{\partial V}{\partial y}\right)^{2} + \left(\frac{\partial W}{\partial y}\right)^{2} \\ \gamma_{xy}^{NL} &= \left(\frac{\partial U}{\partial x}\right)\left(\frac{\partial U}{\partial y}\right) + \left(\frac{\partial V}{\partial x}\right)\left(\frac{\partial V}{\partial y}\right) + \left(\frac{\partial W}{\partial x}\right)\left(\frac{\partial W}{\partial y}\right) \end{aligned} \tag{17}$$

The strain energy of the heated composite laminated plate can be written as

$$U_{e} = \frac{1}{2}\int_{x=0}^{a}\int_{y=0}^{b}\left(N_{x}\varepsilon_{x}^{0} + N_{y}\varepsilon_{y}^{0} + N_{xy}\gamma_{xy}^{0} + M_{x}\chi_{x} + M_{y}\chi_{y} + M_{xy}\chi_{xy} + Q_{y}\gamma_{yz} + Q_{x}\gamma_{xz}\right)dxdy + \frac{1}{2}\int_{x=0}^{a}\int_{y=0}^{b}\sum_{k=1}^{N_{L}}\int_{z=Z_{k}}^{Z_{k+1}}\left(\sigma_{x}^{Tk}\varepsilon_{x}^{NL} + \sigma_{y}^{Tk}\varepsilon_{y}^{NL} + 2\tau_{xy}^{Tk}\gamma_{xy}^{NL}\right)dzdxdy \tag{18}$$

The kinetic energy of the plate can be written as

$$T = \frac{1}{2}\int_{x=0}^{a}\int_{y=0}^{b}\left[I_{0}(\dot{u}^{2}+\dot{v}^{2}+\dot{w}^{2}) + 2I_{1}(\dot{u}\dot{\psi}_{x}+\dot{v}\dot{\psi}_{y}) + I_{2}(\dot{\psi}_{x}^{2}+\dot{\psi}_{y}^{2})\right]dxdy \tag{19}$$

where the symbol ($\dot{\ }$) represent $\partial/\partial t$. The thickness of the plate varies in x-direction, therefore, inertia item I_i are expressed as

$$I_0 = \sum_{k=1}^{N_L} \frac{\rho h_0}{N_L}\left[1-\eta\left(\frac{x}{a}\right)^p\right]$$
$$I_1 = \frac{1}{2}\sum_{k=1}^{N_L} \rho h_0^2\left[1-\eta\left(\frac{x}{a}\right)^p\right]^2\left[\left(\frac{k}{N_L}-0.5\right)^2-\left(\frac{k-1}{N_L}-0.5\right)^2\right] \quad (20)$$
$$I_2 = \frac{1}{2}\sum_{k=1}^{N_L} \rho h_0^3\left[1-\eta\left(\frac{x}{a}\right)^p\right]^3\left[\left(\frac{k}{N_L}-0.5\right)^3-\left(\frac{k-1}{N_L}-0.5\right)^3\right]$$

where ρ is the density of the composite laminated plate.

In this study, the artificial spring technique is introduced to enforce the boundary conditions. That is, the elastic energy stored in four bounds of the plate is expressed as

$$U_b = \frac{1}{2}\int_{y=0}^{b}\left[\begin{array}{l}\left(k_{u0}^x u^2 + k_{v0}^x v^2 + k_{w0}^x w^2 + k_{x0}^x \psi_x^2 + k_{y0}^x \psi_y^2\right)_{x=0} + \\ \left(k_{u1}^x u^2 + k_{v1}^x v^2 + k_{w1}^x w^2 + k_{x1}^x \psi_x^2 + k_{y1}^x \psi_y^2\right)_{x=a}\end{array}\right]dy$$
$$+\frac{1}{2}\int_{x=0}^{a}\left[\begin{array}{l}\left(k_{u0}^y u^2 + k_{v0}^y v^2 + k_{w0}^y w^2 + k_{x0}^y \psi_x^2 + k_{y0}^y \psi_y^2\right)_{y=0} + \\ \left(k_{u1}^y u^2 + k_{v1}^y v^2 + k_{w1}^y w^2 + k_{x1}^y \psi_x^2 + k_{y1}^y \psi_y^2\right)_{y=b}\end{array}\right]dx \quad (21)$$

where k_{ui}^j, k_{vi}^j and k_{wi}^j (i=0,1; j=x,y) indicate the stiffness values of the three linear springs distributed alone the bounds $j=j_i$. k_{xi}^j and k_{yi}^j are the stiffness values of the two rotational springs.

The work done by the external excitation can be written as

$$W_e = \int_{x=0}^{a}\int_{y=0}^{b} pwdxdy \quad (22)$$

where p is the stationary stochastic excitation exerted on the plate surface.

The total Lagrangian energy function of the heated composite laminated plate can be expressed as

$$L = T - U_e - U_b + W_e \quad (23)$$

According to Hamilton's principle,

$$\delta\int_0^t \left(T - U_e - U_b + W_e\right)dt = 0 \quad (24)$$

Substituting Eqs. (18)~(23) into Eq. (24), the governing equations and boundary conditions for the heated composite laminated plate are obtained as follows.

$$\boldsymbol{m}\ddot{\boldsymbol{u}} + \boldsymbol{k}\boldsymbol{u} = \boldsymbol{f} \quad (25)$$

$$\begin{array}{l}\boldsymbol{c}_x\boldsymbol{u} = \boldsymbol{0} \quad : \quad x = 0, a \\ \boldsymbol{c}_y\boldsymbol{u} = \boldsymbol{0} \quad : \quad y = 0, b\end{array} \quad (25)$$

where the mass matrix $\boldsymbol{m}$ and force vector $\boldsymbol{f}$ are as

$$\boldsymbol{m} = \begin{bmatrix} -I_0 & 0 & 0 & -I_1 & 0 \\ 0 & -I_0 & 0 & 0 & -I_1 \\ 0 & 0 & -I_0 & 0 & 0 \\ -I_1 & 0 & 0 & -I_2 & 0 \\ 0 & -I_1 & 0 & 0 & -I_2 \end{bmatrix} \quad (26)$$

$$\boldsymbol{f} = \begin{bmatrix} 0 & 0 & -p & 0 & 0 \end{bmatrix}^T \tag{27}$$

The detailed components of the matrices $\boldsymbol{k}$, $\boldsymbol{c}_x$ and $\boldsymbol{c}_y$ are shown in Appendices A~C, respectively.

Meshfree Jacobi point interpolation (MJPI) shape function

In this study, a MJPI shape function using the Jacobi polynomials as the basis is presented and applied to approximate the displacement components of the heated plate with varying thickness and curvilinear fiber. For a point (x,y) in the two-dimensional domain, MJPI approximation of displacement $u(x,y)$ can be defined as

$$u(x,y) = \sum_{i=1}^{m} J_i(x,y) a_i = \boldsymbol{J}(x,y)\boldsymbol{a} \tag{29}$$

where $J_i(x,y)$ and m denote Jacobi polynomial basis and number of basis.

In the two-dimensional Jacobi polynomial basis can be obtained from Kronecker product of one-dimensional basis.

$$\boldsymbol{J}(x,y) = \begin{bmatrix} J_1(x) & \cdots & J_j(x) & \cdots \end{bmatrix} \otimes \begin{bmatrix} J_1(y) & \cdots & J_j(y) & \cdots \end{bmatrix} \tag{30}$$

One-dimensional Jacobi polynomial is expressed as

$$\begin{cases} J_1(x) = 1, \quad J_2(x) = \dfrac{1}{2}(\alpha+\beta+2)x + \dfrac{1}{2}(\alpha-\beta) \\ J_i(x) = \dfrac{\begin{Bmatrix} (2i+\alpha+\beta-1)[(2i+\alpha+\beta)(2i+\alpha+\beta-2)x + \alpha^2 - \beta^2]J_{i-1}(x) \\ -2(i+\alpha-1)(i+\beta-1)(2i+\alpha+\beta)J_{i-2}(x) \end{Bmatrix}}{2i(i+\alpha+\beta)(2i+\alpha+\beta-2)} \quad i = 3,4,\cdots \end{cases} \tag{31}$$

where $\alpha, \beta > -1$. If $\alpha, \beta = 0$, the above equation represents the Legendre polynomial.

In order to determine the unknown coefficients a_i, Eq. (29) is applied to all nodes distributed in two-dimensional problem domain. That is,

$$\boldsymbol{u}_s = \boldsymbol{J}_m \boldsymbol{a} \tag{32}$$

Where

$$\boldsymbol{u}_s = \begin{bmatrix} u_1 & u_2 & \cdots & u_N \end{bmatrix}^T \tag{33}$$

$$\boldsymbol{a} = \begin{bmatrix} a_1 & a_2 & \cdots & a_m \end{bmatrix}^T \tag{34}$$

$$\boldsymbol{J}_m = \begin{bmatrix} \boldsymbol{J}(x_1,y_1) & \boldsymbol{J}(x_2,y_2) & \cdots & \boldsymbol{J}(x_N,y_N) \end{bmatrix}^T \tag{35}$$

where N denotes the number of nodes.

If the number of basis m is the same as the number of nodes N, then J_m is a square matrix. From Eq. (32), the unknown coefficient matrix can be obtained as

$$\boldsymbol{a} = \boldsymbol{J}_m^{-1} \boldsymbol{u}_s \tag{36}$$

Substituting Eq. (36) into Eq. (29)

$$u(x,y) = \boldsymbol{J}(x,y)\boldsymbol{J}_m^{-1}\boldsymbol{u}_s = \sum_{i=1}^{N} \phi_i(x,y) u_i = \tilde{\boldsymbol{\Phi}}(x,y)\boldsymbol{u}_s \tag{37}$$

where $\tilde{\boldsymbol{\Phi}}(x,y)$ is the MJPI shape function vector.

$$\tilde{\boldsymbol{\Phi}}(x,y) = \boldsymbol{J}(x,y)\boldsymbol{J}_m^{-1} = \begin{bmatrix} \phi_1(x,y) & \phi_2(x,y) & \cdots & \phi_N(x,y) \end{bmatrix} \tag{38}$$

2.4 Discretized equations of motion

The displacement components of a node *I* distributed in the composite laminated plate are approximated by the MJPI shape function as

$$\begin{aligned}\boldsymbol{u}(x_I,y_I)&=\left[u(x_I,y_I)\quad v(x_I,y_I)\quad w(x_I,y_I)\quad \psi_x(x_I,y_I)\quad \psi_y(x_I,y_I)\right]^T\\&=\boldsymbol{\Phi}(x_I,y_I)\boldsymbol{U}_s\end{aligned} \tag{39}$$

The expanded MJPI shape function $\Phi(x_I,y_I)$ is expressed as

$$\boldsymbol{\Phi}(x_I,y_I)=\left[\boldsymbol{\Phi}_1(x_I,y_I)\quad \boldsymbol{\Phi}_2(x_I,y_I)\quad \cdots\quad \boldsymbol{\Phi}_i(x_I,y_I)\quad \cdots\quad \boldsymbol{\Phi}_N(x_I,y_I)\right] \tag{40}$$

Where

$$\boldsymbol{\Phi}_i(x_I,y_I)=diag\left[\phi_i(x_I,y_I)\quad \phi_i(x_I,y_I)\quad \phi_i(x_I,y_I)\quad \phi_i(x_I,y_I)\quad \phi_i(x_I,y_I)\right] \tag{41}$$

Similarly, the total displacement vector $\boldsymbol{U}_s$ can be written as

$$\boldsymbol{U}_s=\left[u_1\quad v_1\quad w_1\quad \psi_{x1}\quad \psi_{y1}\quad \cdots\quad u_N\quad v_N\quad w_N\quad \psi_{xN}\quad \psi_{yN}\right]^T \tag{42}$$

Substituting Eq. (39) into Eq. (25) and assuming harmonic motion, the nodal equation of motion is obtained as

$$\left(\boldsymbol{k}_I-\omega^2\boldsymbol{m}_I\right)\boldsymbol{U}_s=\boldsymbol{f}_I \tag{43}$$

where ω is the natural frequency of the heated composite laminated plate with varying thickness and curvilinear fiber.

The nodal mass matrix m_I, nodal stiffness matrix $\boldsymbol{k}_I$ and nodal force vector $\boldsymbol{f}_I$ are as

$$\boldsymbol{m}_I=\boldsymbol{m}\boldsymbol{\Phi}(x_I,y_I),\quad \boldsymbol{k}_I=\boldsymbol{k}\boldsymbol{\Phi}(x_I,y_I),\quad \boldsymbol{f}_I=\boldsymbol{f}(x_I,y_I) \tag{44}$$

The discretized equations of motion for the composite laminated plate are obtained by grouping the nodal equations for all nodes distributed in problem domain. That is,

$$\left(\boldsymbol{K}-\omega^2\boldsymbol{M}\right)\boldsymbol{U}_s=\boldsymbol{F} \tag{45}$$

Where

$$\boldsymbol{K}=\left[\boldsymbol{k}_1\quad \boldsymbol{k}_2\quad \cdots\quad \boldsymbol{k}_N\right]^T \tag{46}$$

$$\boldsymbol{M}=\left[\boldsymbol{m}_1\quad \boldsymbol{m}_2\quad \cdots\quad \boldsymbol{m}_N\right]^T \tag{47}$$

$$\boldsymbol{F}=\left[\boldsymbol{f}_1\quad \boldsymbol{f}_2\quad \cdots\quad \boldsymbol{f}_N\right]^T \tag{48}$$

Similarly, the discretized boundary conditions can be obtained by substituting Eq. (39) into Eq. (26).

$$\begin{aligned}&\boldsymbol{c}_x\boldsymbol{\Phi}(x_I,y_I)\boldsymbol{U}_s=\boldsymbol{0}\quad :\quad x=0,a\\&\boldsymbol{c}_y\boldsymbol{\Phi}(x_I,y_I)\boldsymbol{U}_s=\boldsymbol{0}\quad :\quad y=0,b\end{aligned} \tag{49}$$

In this study, a band-limited base acceleration with PSD function S_0=0.5g^2/Hz is assumed as stationary stochastic excitation. When the composite plate is subjected to the band-limited base acceleration, the detailed stochastic excitation can be given as

$$p=-I_0\sqrt{S_0}e^{i\omega t} \tag{50}$$

The stochastic response of the plate structure with the damping ratio are evaluated by using the auto-PSD functions as

$$\begin{cases}S_w(x,y,\omega)=w(x,y,\omega)*w(x,y,\omega)\\S_{\dot{w}}(x,y,\omega)=\omega^2S_w\\S_{\ddot{w}}(x,y,\omega)=\omega^4S_w\end{cases} \tag{51}$$

Where S_w, $S_{\dot{w}}$ and $S_{\ddot{w}}$ denote the displacement, velocity and acceleration PSD functions for stationary random transverse responses. The symbol $(*)$ in the above equation indicates the complex conjugate.
For a stationary stochastic excitation within frequency interval $[\omega_0, \omega_1]$, the root mean square (RMS) of the responses can be written as

$$R_{\bar{w}}(x,y)=\sqrt{\int_{\omega_0}^{\omega_1} S_{\bar{w}}(x,y,\omega)d\omega}, \quad \bar{w}=w,\dot{w},\ddot{w} \tag{52}$$

Numerical results and discussions

In this section, the accuracy and reliability of the presented method are verified by convergence study and comparing of the frequency parameters for different laminated plates obtained using the presented method with the results of literatures and finite element software ABAQUS. Numerical examples of free vibration and stochastic response for heated composite laminated plates with varying thickness and curvilinear fiber are provided. Numerical results by the presented method are provided through self-compiled MATLAB code. Unless otherwise stated, the material properties of composite laminated composite plates used in numerical examples are as E_1=150GPa, E_2=10GPa, μ=0.25, G_{12}=G_{13}=6GPa, G_{23}=5GPa, ρ=1500kg/m^2, α_{11}=7×10^{-6}K^{-1}, α_{22}=2.3×10^{-5}K^{-1} and α_{12}=0. Table 1 shows the stiffness values of the artificial springs for clamped (C), free (F) and simply supported (S) boundaries.

Table 1: Spring stiffness values of ground for classical boundary conditions (i=0, 1).

Boundary condition	$k_{ui}^x(=k_{ui}^y)$	$k_{vi}^x(=k_{vi}^y)$	$k_{wi}^x(=k_{wi}^y)$	k_{xi}^x	k_{xi}^y	k_{yi}^x	k_{yi}^y
F (free)	0	0	0	0	0	0	0
S (simply supported)	10^{14}	10^{14}	10^{14}	0	10^{14}	10^{14}	0
C (clamped)	10^{14}	10^{14}	10^{14}	10^{14}	10^{14}	10^{14}	10^{14}

Verification and convergence study

Firstly, the convergence of the stiffness values of the artificial springs is investigated. The left edge of composite laminated plate is selected as the elastic boundary, and the other boundary is clamped. Fig. 2 illustrates the variation of the frequency parameters $\Omega=\omega a^2\sqrt{\rho/E_2h_0^2}$ for the plate with varying thickness and curvilinear fiber according to the spring stiffness values of the elastic boundary. The geometric dimensions of the plate are as a=b=1m, h_0=0.05m, λ=π/4, η=0.5, p=1, and the initial fiber directions are as [0˚/45˚/0˚]. The plate is affected by the temperature difference ΔT=20K. As can be seen in Fig. 2, the frequency parameters in the stiffness value interval of 10^5 ~ 10^{11} increase faster than those of the other intervals. When the stiffness values are higher than 10^{13} or lower than 10^3, the frequencies tend to be stable. It means that the clamped boundary and free boundary can be simulated by assuming the stiffness value equal to infinity and zero, respectively. As shown in Table 1, the stiffness value for the clamped boundary is selected as 10^{14} in this study.

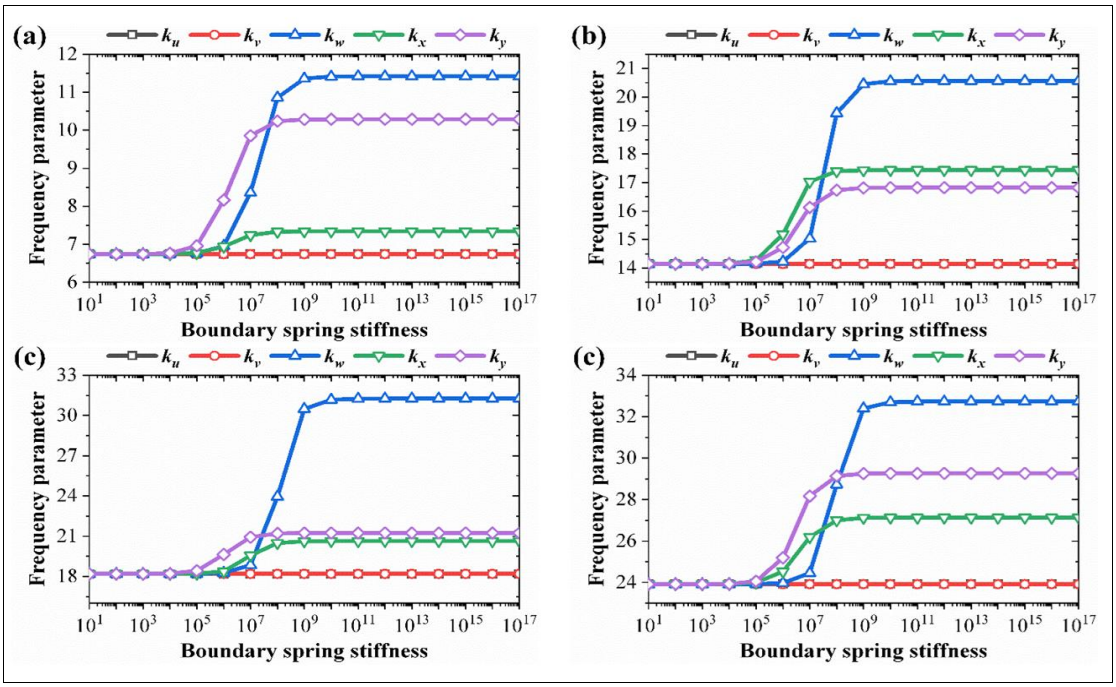

Fig 2: Variation of frequency parameters of heated composite laminated plate with varying thickness and curvilinear fiber on boundary spring stiffness; (a) Mode 1 (b) Mode2 (c) Mode 3 (d) Mode 4.

For the same plate, the convergence of frequency parameters according to the number of nodes distributed in *x*-direction of the plate is investigated. In this study, the problem domain is discretized by *N* nodes distributed regularly, and the same number of nodes is selected in *x*- and y-directions of the plate. It can be seen from Fig. 3 that as the number of nodes in *x*-direction increased the lowest four frequencies of the composite laminated plate with different boundary conditions converges, and the frequency solutions are relatively stable when the number of nodes exceeds 10.

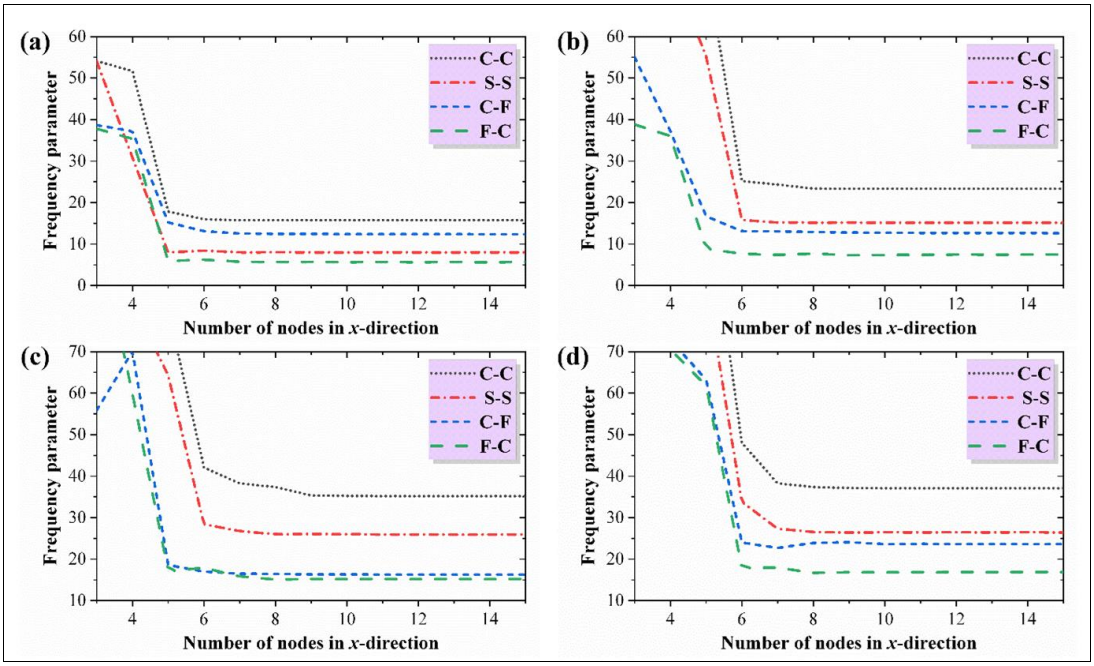

Fig 3: Variation of frequency parameters of heated composite laminated plate with varying thickness and curvilinear fiber on number of nodes; (a) Mode 1 (b) Mode 2 (c) Mode 3 (d) Mode 4.

Subsequently, in order to confirm the accuracy of the presented method, the frequency parameters of different plates obtained by the presented method are compared with those of literatures and FEM. Table 2 shows the comparison of lowest five frequency parameters $\Omega = \omega a^2\sqrt{\rho/E_2h^2}$ of an angle-ply [-45˚/45˚] plate with uniform thickness and fiber angle. The material properties and geometric dimensions of the plate are as E_1/E_2=40, μ=0.25, $G_{12}=G_{13}=0.5E_2$, $G_{23}=0.2E_2$ and a/b=1. Besides, the comparison of natural frequencies for heated composite laminated plate with uniform thickness and fiber angle is illustrated in Table 3. The material properties and geometric dimensions are as E_1=175GPa, E_2=32GPa, μ=0.25, $G_{12}=G_{13}$=12GPa, G_{23}=5.7GPa, ρ=1760kg/m^2, $\alpha_{11}=1.2\times10^{-6}$K^{-1}, $\alpha_{22}=2.3\times10^{-6}$K^{-1}, α_{12}=0, $a=b$=1m, h=0.01m and ΔT=20K. From the comparisons in the tables 2 and 3, it is obvious that the present results agree very well with FSDT solutions reported by Ye *et al.* [21] and by Zhou *et al.* [43].

Table 2: Comparison of frequency parameters for an angle-ply plate with uniform thickness and fiber angle.

Boundary condition	Ω	h								
		0.05			0.1			0.2		
		Ref.[21]	Present	Diff, %	Ref.[21]	Present	Diff, %	Ref.[21]	Present	Diff, %
FCFC	1	11.201	11.202	-0.009	9.6505	9.6481	0.025	6.8492	6.8485	0.010
	2	15.397	15.426	-0.188	12.729	12.726	0.024	8.8625	8.8627	-0.002
	3	26.651	26.652	-0.004	21.040	21.041	-0.005	14.047	14.049	-0.014
	4	29.036	29.044	-0.028	22.431	22.431	0.000	14.140	14.141	-0.007
	5	34.400	34.477	-0.224	26.105	26.105	0.000	16.347	16.349	-0.012
SSSS	1	17.162	17.165	-0.017	14.509	14.514	-0.034	9.9864	9.9905	-0.041
	2	33.350	33.354	-0.012	26.115	26.121	-0.023	16.560	16.564	-0.024
	3	33.350	33.354	-0.012	26.115	26.121	-0.023	16.560	16.564	-0.024
	4	52.917	52.920	-0.006	38.013	38.019	-0.016	22.332	22.336	-0.018
	5	53.295	53.285	0.019	39.556	39.552	0.010	24.120	24.121	-0.004
CCCC	1	20.460	20.460	0.000	16.219	16.220	-0.006	10.482	10.483	-0.010
	2	38.541	38.542	-0.003	28.201	28.202	-0.004	16.970	16.972	-0.012
	3	38.541	38.542	-0.003	28.201	28.202	-0.004	16.970	16.972	-0.012
	4	56.750	56.750	0.000	39.024	39.026	-0.005	22.474	22.476	-0.009
	5	61.840	61.843	-0.005	42.362	42.364	-0.005	24.496	24.499	-0.012

Table 3: Comparison of natural frequencies for heated composite laminated plate with uniform thickness and fiber angle.

Lamination	ω	SSSS			SCSC			CCCC		
		Ref.[43]	Present	Diff, %	Ref.[43]	Present	Diff, %	Ref.[43]	Present	Diff, %

[0˚/0˚/0˚/ 0˚/0˚]	1	47.991	47.908	0.173	63.062	63.028	0.054	111.85	111.85	0.000
	2	97.616	97.314	0.309	135.80	135.73	0.052	165.97	165.90	0.042
	3	182.86	182.67	0.104	188.41	188.36	0.027	269.28	269.14	0.052
	4	191.13	190.72	0.215	239.74	239.61	0.054	286.66	286.61	0.017
	5	217.82	217.25	0.262	250.24	250.06	0.072	324.98	324.87	0.034
	6	292.73	291.75	0.335	336.86	336.58	0.083	404.71	404.50	0.052
[45˚/-45˚/45˚/ -45˚/45˚]	1	60.821	60.520	0.495	86.368	86.342	0.030	106.58	106.55	0.028
	2	139.90	139.84	0.043	164.22	164.10	0.073	205.76	205.63	0.063
	3	163.37	162.41	0.588	209.02	208.83	0.091	230.96	230.82	0.061
	4	245.05	244.77	0.114	280.72	280.51	0.075	325.54	325.24	0.092
	5	291.06	290.96	0.034	320.39	319.98	0.128	382.01	381.68	0.086
	6	311.89	310.01	0.603	381.68	381.25	0.113	402.48	402.06	0.104
[0˚/90˚/0˚/ 90˚/0˚]	1	48.071	47.906	0.343	73.365	73.353	0.016	111.88	111.87	0.009
	2	119.52	119.23	0.243	176.25	176.17	0.045	196.85	196.79	0.030
	3	169.39	169.19	0.118	179.46	179.41	0.028	266.53	266.48	0.019
	4	217.84	217.23	0.280	255.73	255.61	0.047	325.09	324.99	0.031
	5	251.13	250.73	0.159	335.50	335.31	0.057	347.82	347.71	0.032
	6	327.80	326.83	0.296	379.29	379.09	0.053	448.34	448.14	0.045

In order to further validate the accuracy of the present method, the frequency parameters $\Omega = \omega a^2\sqrt{\rho/E_2 h_0^2}$ of heated composite laminated plate with varying thickness and curvilinear fiber obtained by the current method are compared with those from finite element software ABAQUS in Table 4. The initial fiber angle of the plate is [0˚/45˚/0˚], and other geometric dimensions are as a=1.5m, b=1m, h_0=0.1m, p=1 and $\lambda=\pi/6$. The composite laminated plate is subjected to thermal load ΔT=20K, and the material properties are the same as in previous example. In the case of FEM software ABAQUS, 9600 S4R elements are used. It can be seen from Table 4 that the differences of the frequency results between the current method and ABAQUS are less than 1%. The comparisons of lowest four mode shapes of the plates with CCCC and FCFC boundary conditions are shown in Figs 4 and 5, respectively.

Table 4: Comparison of frequency parameters for heated composite laminated plate with varying thickness and curvilinear fiber.

η	Ω	SSSS			FCFC			CCCC		
		FEM	Present	Diff, %	FEM	Present	Diff, %	FEM	Present	Diff, %
-0.5	1	14.698	14.752	-0.367	15.722	15.616	0.674	22.858	22.991	-0.582
	2	29.643	29.722	-0.267	20.489	20.389	0.488	36.963	36.809	0.417
	3	35.290	35.306	-0.045	27.708	27.750	-0.152	44.938	44.727	0.470
	4	45.838	45.971	-0.290	36.459	36.335	0.340	52.678	52.708	-0.057
0	1	12.024	12.045	-0.175	14.184	14.084	0.705	19.718	19.809	-0.462
	2	24.883	25.101	-0.876	16.656	16.582	0.444	32.452	32.555	-0.317
	3	30.561	30.516	0.147	23.429	23.426	0.013	40.276	40.053	0.554
	4	39.258	39.565	-0.782	34.177	34.150	0.079	47.233	47.150	0.176
0.5	1	8.8543	8.8581	-0.043	10.830	10.759	0.656	15.375	15.412	-0.241
	2	18.958	19.037	-0.417	13.220	13.152	0.514	26.062	26.146	-0.322
	3	23.912	23.830	0.343	18.040	17.994	0.255	32.669	32.486	0.560
	4	30.686	30.763	-0.251	27.031	26.998	0.122	38.337	38.614	-0.723

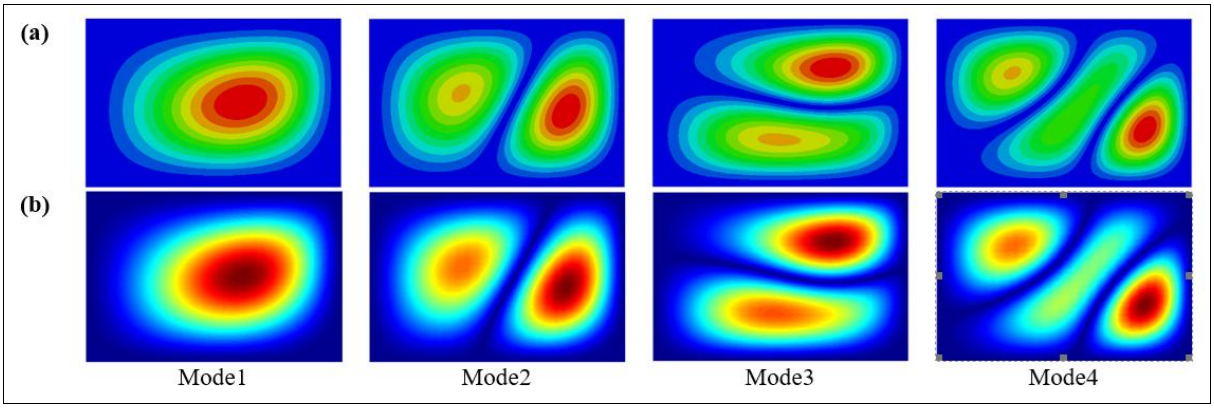

Fig 4: Mode shapes of heated composite laminated plate with varying thickness and fiber angle under CCCC boundary condition (η=0.5); (a) FEM (b) Present.

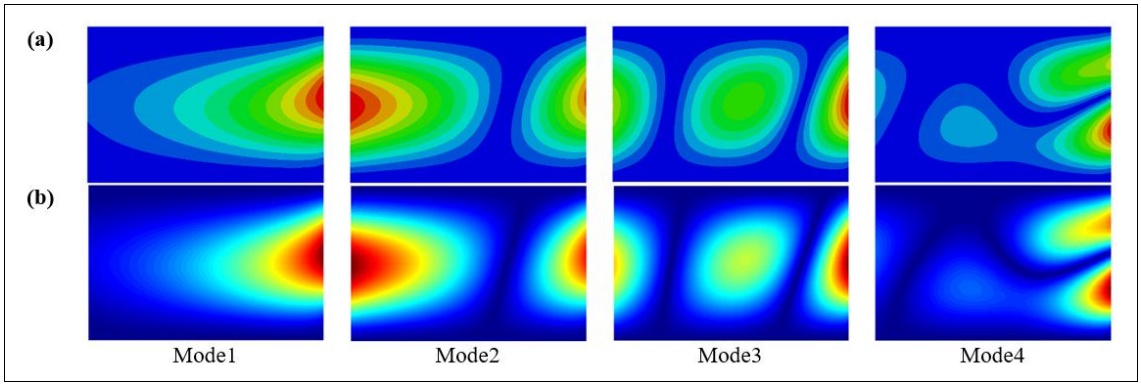

Fig 5: Mode shapes of heated composite laminated plate with varying thickness and fiber angle under FCFC boundary condition (η=0.5); (a) FEM (b) Present.

In Table 5, the displacement, velocity and acceleration RMS responses of a isotropic plate excited by the band-limited base acceleration within the frequency interval [20, 2000] Hz are compared. The material properties and the geometric dimensions are given as E=70GPa, μ=0.33, ρ=2700kg/m^2, a=0.4m, b=0.2m and h=0.002m. The damping ratio of the plate is selected as 0.05 and the RMS responses are evaluated at the center of the plate. As can be seen from Table 5, the RMS response results by the current method are well consistent with those of literature. Subsequently, for a composite laminated [0˚/90˚/0˚] plate with varying thickness excited by the band-limited base acceleration, displacement and acceleration response curves plotted by the current method are compared with those from ABAQUS in Fig. 6. In this example, the damping ratio is neglected and the response results are evaluated at the center of the plate. The material properties of the plate are the same as in Table 3, and the geometric dimensions are as a=2m, b=1m, h_0=0.05m, η=0.5 and p=1. From the above comparisons, it is observed that the present method is reliable and capable of handling the dynamic problems of heated composite laminated plate with varying thickness and curvilinear fiber.

Table 5: Root mean square of responses for isotropic plate subjected to stationary random excitation.

Boundary condition	Root mean square of responses								
	Displacement, m			Velocity, m/s			Acceleration, m/s^2		
	CPT [44]	Present	Diff. %	CPT[44]	Present	Diff. %	CPT[44]	Present	Diff. %
SSSS	5.994×10^{-4}	5.974×10^{-4}	0.334	0.591	0.592	-0.169	929.13	927.29	0.198
SSSC	3.523×10^{-4}	3.530×10^{-4}	-0.199	0.491	0.493	-0.407	989.22	989.96	-0.075
SCSC	2.320×10^{-4}	2.331×10^{-4}	-0.474	0.447	0.449	-0.447	1220.66	1213.89	0.555

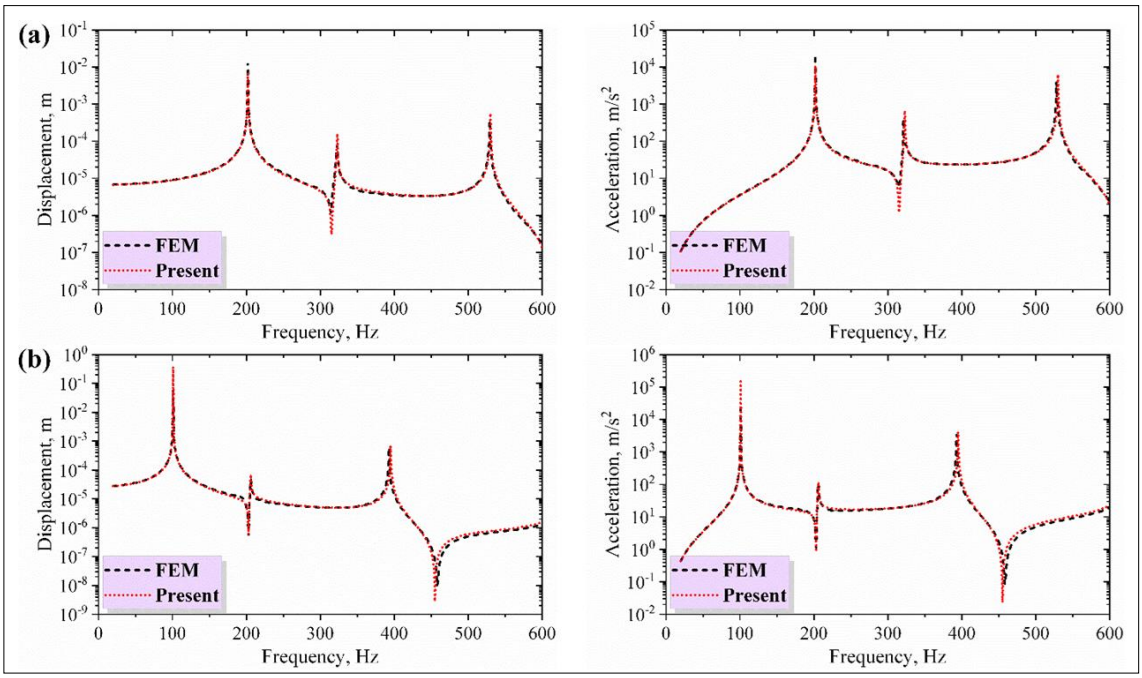

Fig 6: Displacement and acceleration response curves of composite laminated plate with varying thickness subjected to stationary random excitation; (a) CCCC (b) SSSS.

Parametric study

Based on the verification of reliability and accuracy of the presented method, the parametric study on the free vibration and stochastic response of heated composite laminated plates with varying thickness and curvilinear fiber is performed.

Firstly, the effect of the thickness gradient η and power index p on the frequency parameter $\Omega = \omega a^2\sqrt{\rho/E_2 h_0^2}$ of heated composite laminated plate with curvilinear fiber is investigated in Fig. 7. The geometric dimensions of the plate are as a=b=1m, h_0=0.05m, λ=π/4. The plate is affected by thermal load ΔT=20K, and the initial fiber angle is chosen as [0˚/45˚/0˚]. As can be seen from Fig. 7, the frequency parameters decrease as the thickness gradient η increases regardless of mode number, thickness power index and boundary condition. It means that the stiffness of the plate structure decreases as the thickness gradient increases. The frequency parameters of the plates with positive thickness gradient increase as the thickness power index p increases regardless of boundary condition and mode number, and in the case of negative thickness gradient, it is opposite. It is because the second term $(x/a)^p$ of Eq. (1) decreases as thickness index p increases.

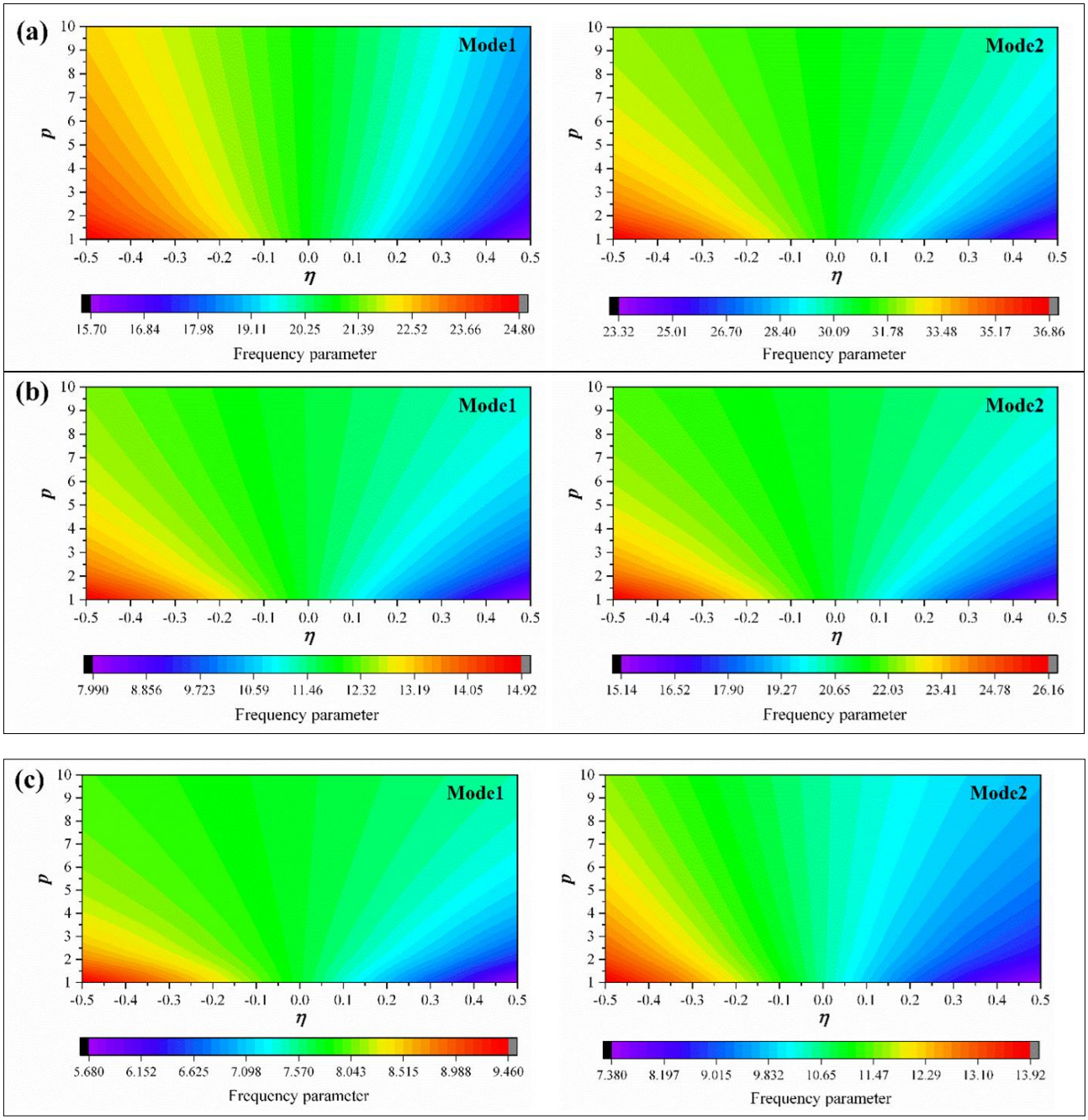

Fig 7: Variation of frequency parameters of heated composite laminated plate with different thickness gradients and power indices; (a) CCCC (b) SSSS (c) FCFC.

Next, the effect of fiber direction coefficient and initial fiber angle on the frequency parameter Ω of heated composite plate with varying thickness is investigated. The composite laminated plate is subjected to thermal load ΔT=20K, and the geometric dimensions are taken to be a=b=1m, h_0=0.05m, η=0.5 and p=1. The variation of lowest four frequencies of clamped plate with initial fiber angle [0˚/θ˚/0˚] according to the angle θ and fiber direction coefficient λ is depicted in Fig. 8.

As can be seen from Fig. 8, first and fourth frequencies of the composite laminated plate decrease as the fiber direction coefficient increases regardless of the initial fiber angle θ. In other words, the first and fourth frequency parameters of the composite laminated plate with curvilinear fiber are lower than those of linear fiber (λ=0). When the angle θ is less than π/4, the second and third frequencies increase as the fiber direction coefficient increases. However, in the case that the angle θ is

greater than $\pi/4$, it is opposite. It is obvious that the effect of fiber direction coefficient on the frequencies of the clamped composite plate depends on the mode number and initial fiber angle. Similarly, the effect of the fiber direction coefficient and initial fiber angle on the frequency parameters of heated composite laminated plates with SSSS and FCFC boundary conditions is exhibited in Tables 6 and 7, which may serve as reference data.

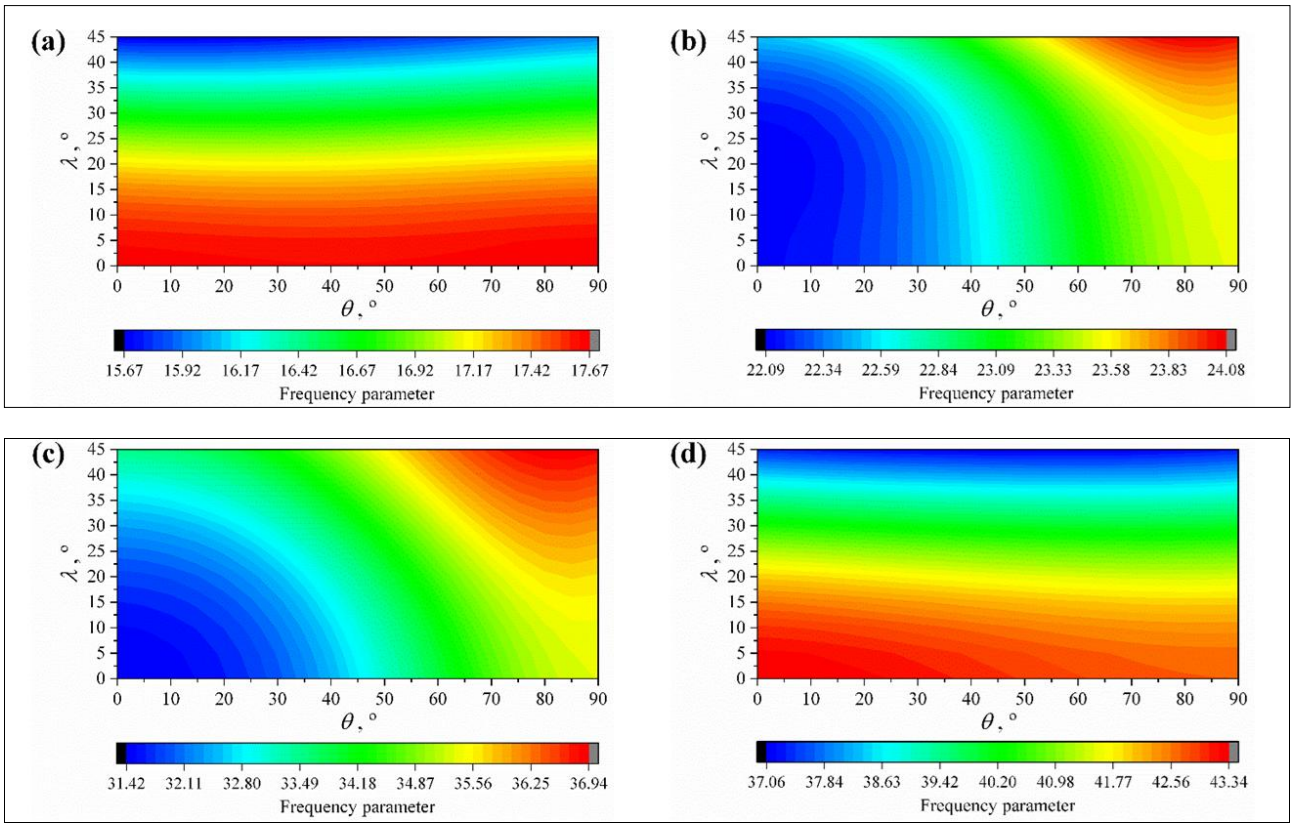

Fig 8: Variation of frequency parameters of heated composite laminated plate with different fiber direction coefficients under CCCC boundary condition; (a) Mode 1 (b) Mode 2 (c) Mode 3 (d) Mode 4.

Table 6: Frequency parameters of heated composite laminated plate with different fiber direction coefficients under SSSS boundary condition.

Initial lamination	**Ω**	**λ, °**									
		0	**5**	**10**	**15**	**20**	**25**	**30**	**35**	**40**	**45**
[0˚/30˚/0˚]	1	8.375	8.365	8.347	8.321	8.287	8.243	8.190	8.129	8.061	7.987
	2	13.269	13.297	13.376	13.502	13.669	13.869	14.095	14.340	14.597	14.860
	3	22.712	22.784	22.949	23.194	23.501	23.849	24.215	24.579	24.923	25.233
	4	30.541	30.458	30.268	29.975	29.584	29.103	28.540	27.905	27.212	26.481
[0˚/45˚/0˚]	1	8.406	8.389	8.366	8.336	8.298	8.252	8.198	8.137	8.068	7.993
	2	13.537	13.555	13.625	13.746	13.911	14.114	14.347	14.601	14.868	15.142
	3	23.403	23.483	23.654	23.906	24.219	24.572	24.939	25.297	25.628	25.923
	4	30.452	30.366	30.177	29.886	29.501	29.026	28.472	27.847	27.166	26.448
[0˚/60˚/0˚]	1	8.375	8.354	8.329	8.298	8.262	8.219	8.170	8.116	8.058	7.997
	2	13.748	13.760	13.830	13.955	14.130	14.345	14.593	14.863	15.145	15.431
	3	24.237	24.318	24.492	24.747	25.062	25.412	25.772	26.116	26.430	26.436
	4	30.332	30.252	30.069	29.788	29.412	28.949	28.408	27.800	27.140	26.717
[0˚/90˚/0˚]	1	8.285	8.284	8.282	8.277	8.270	8.260	8.246	8.225	8.198	8.162
	2	13.925	13.957	14.051	14.202	14.403	14.640	14.902	15.175	15.450	15.719
	3	25.252	25.300	25.442	25.664	25.946	26.264	26.590	26.902	27.147	26.647
	4	30.184	30.132	29.980	29.731	29.391	28.968	28.472	27.915	27.350	27.465

Table 7: Frequency parameters of heated composite laminated plate with different fiber direction coefficients under FCFC boundary condition.

Initial lamination	Ω	λ, °									
		0	5	10	15	20	25	30	35	40	45
[0˚/30˚/0˚]	1	4.157	4.183	4.230	4.301	4.400	4.529	4.694	4.899	5.143	5.426
	2	6.061	6.080	6.123	6.189	6.284	6.408	6.562	6.745	6.957	7.204
	3	11.529	11.594	11.708	11.876	12.111	12.430	12.847	13.373	14.001	14.675
	4	16.339	16.344	16.355	16.366	16.371	16.361	16.337	16.302	16.277	16.314
[0˚/45˚/0˚]	1	4.306	4.352	4.416	4.501	4.609	4.748	4.922	5.137	5.392	5.683

	2	6.323	6.334	6.366	6.421	6.503	6.615	6.757	6.932	7.140	7.388
	3	11.928	12.048	12.212	12.424	12.694	13.036	13.463	13.982	14.574	15.153
	4	16.913	16.899	16.888	16.873	16.849	16.811	16.765	16.723	16.720	16.838
[0˚/60˚/0˚]	1	4.512	4.565	4.632	4.718	4.826	4.965	5.140	5.354	5.608	5.896
	2	6.639	6.648	6.677	6.729	6.807	6.916	7.055	7.227	7.431	7.670
	3	12.521	12.662	12.834	13.040	13.293	13.605	13.992	14.457	14.980	15.478
	4	17.749	17.715	17.674	17.619	17.548	17.467	17.385	17.326	17.330	17.479
[0˚/90˚/0˚]	1	4.784	4.789	4.807	4.841	4.899	4.988	5.114	5.283	5.497	5.758
	2	7.052	7.061	7.089	7.140	7.218	7.328	7.469	7.640	7.838	8.061
	3	13.297	13.303	13.324	13.374	13.471	13.637	13.894	14.256	14.721	15.251
	4	18.953	18.903	18.789	18.648	18.497	18.346	18.203	18.084	18.011	18.025

Subsequently, the effect of thermal load on the frequency parameters Ω of composite laminated plates with different thickness gradients is plotted in Fig. 9. The initial fiber angle at the left edge of the plate is as [0˚/45˚/0˚], and the other geometric dimensions are as a=1.5, b=1m, h_0=0.05m, p=1 and $\lambda=\pi/6$. The temperature step is set as 0.5K. In general, the thermal load will significantly soften the stiffness of structures. Therefore, it is clear that the frequency parameters of the plate decrease as the temperature difference increases. Moreover, the decreasing velocity of the frequency parameters of the plate increases as the thickness gradient increases. However, when the temperature difference exceeds the thermal bucking temperature, the frequency parameter increases with the increase of the temperature difference. It can be found that the first and second frequencies of the plate with FCFC boundary condition and η=0.5 are coincided in the frequency interval [201, 215] Hz.

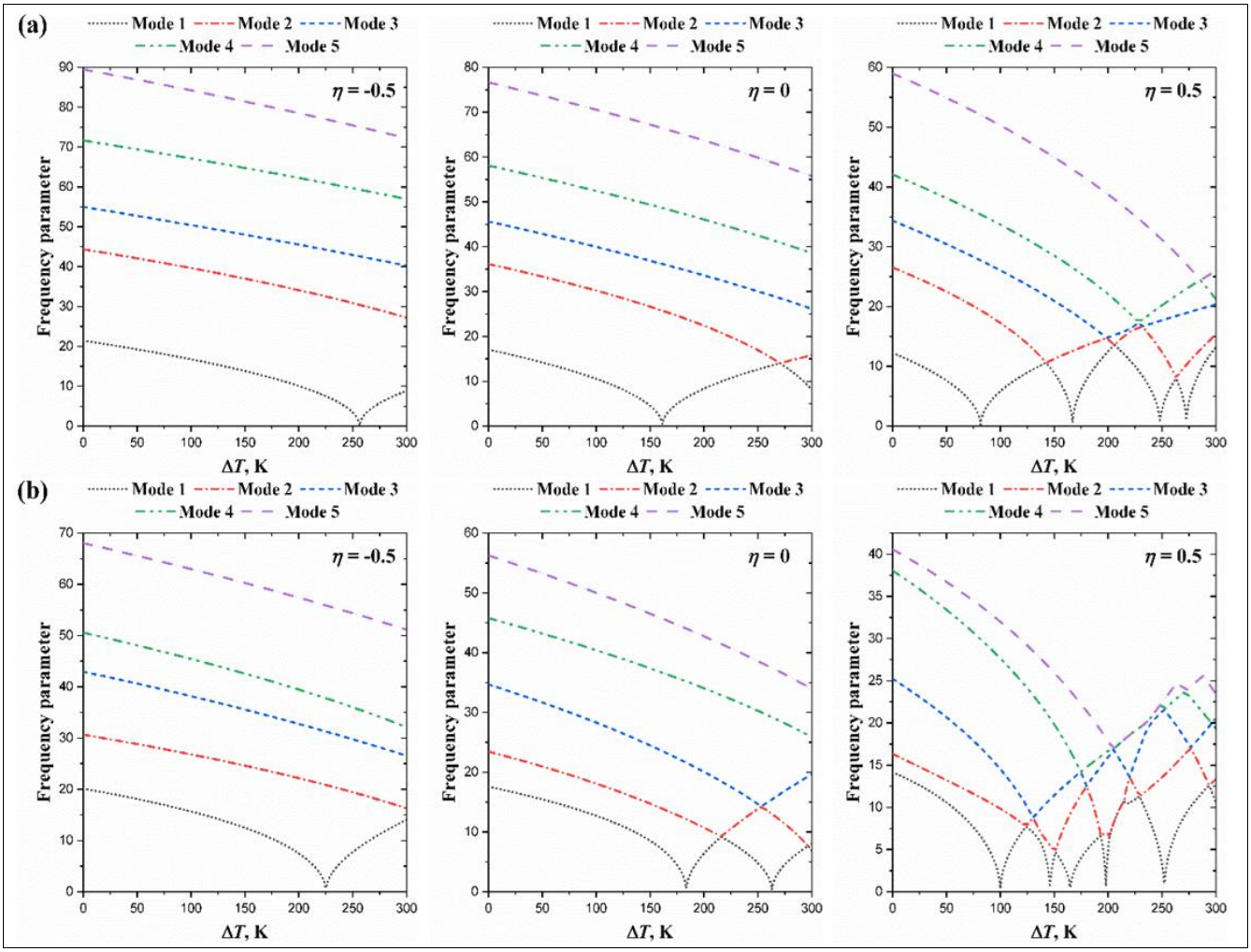

Fig 9: Variation of frequency parameters of composite laminated plate with different thickness gradients and temperature differences; (a) SSSS (b) FCFC.

Besides, Fig. 10 exhibits the relations between the temperature difference and the frequency parameters of composite laminated plate with curvilinear fiber. The thickness gradient is chosen as η=0.5, and other geometric parameters of the plate are the same as previous example. The thermal bucking temperature of the plate with CFCF boundary condition decreases with the increase of the fiber direction coefficient, but the second thermal bucking temperature of clamped plate increases with the increase of the fiber direction coefficient, which means that the thermal bucking temperature of the composite laminated plate with curvilinear fiber depends on the boundary condition and mode number.

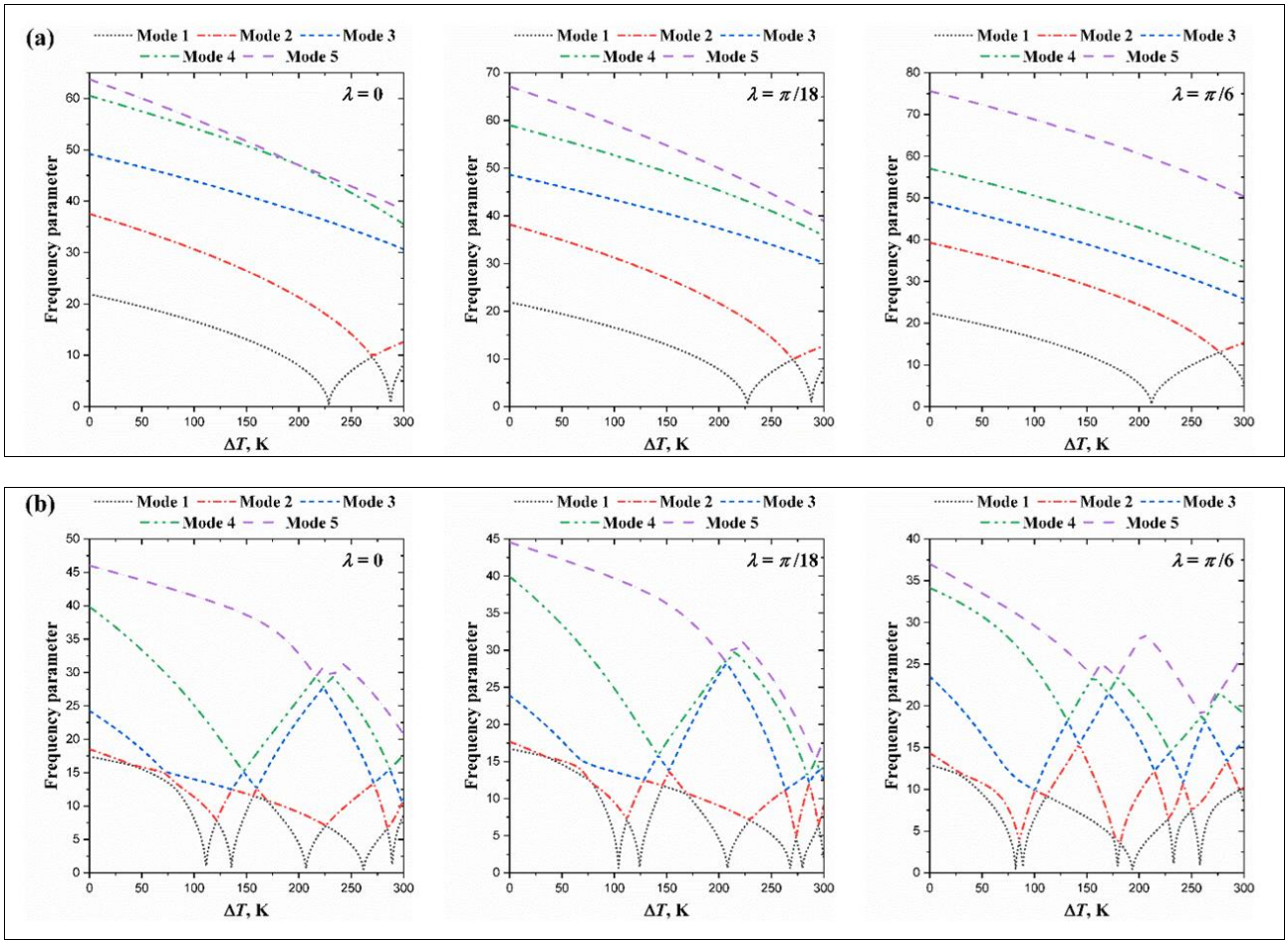

Fig 10: Variation of frequency parameters of composite laminated plate with different fiber direction coefficients and temperature differences; (a) CCCC (b) CFCF.

Next, the effect of thickness gradient and temperature difference on the displacement and acceleration response PSD curves of clamped plate excited by the band-limited base acceleration is plotted in Fig. 11. The geometric dimensions of the plate are the same as in Fig. 9 and mode damping ratio 0.01 is considered. As can be seen from Fig. 11, the peaks of the PSD curves move to lower frequency range with increasing the thickness gradient and temperature difference. In addition, the amplitude of the first pick of the displacement response curves increases with increasing the thickness gradient. It means that the thickness gradient has a more significant effect on the displacement response PSD values than the acceleration response PSD values. Fig. 12 shows the displacement and acceleration RMS responses of the composite laminated plate subjected to the stationary stochastic excitation. In the plate with uniform thickness (η=0), the maximum displacement and maximum acceleration occur at the center point of the plate. However, in the plate with varying thickness, the points where the maximum displacement and maximum acceleration occur move to thinner edge. Moreover, the maximum values of RMS responses of the plate with η=0.5 are greater than those of uniform thickness.

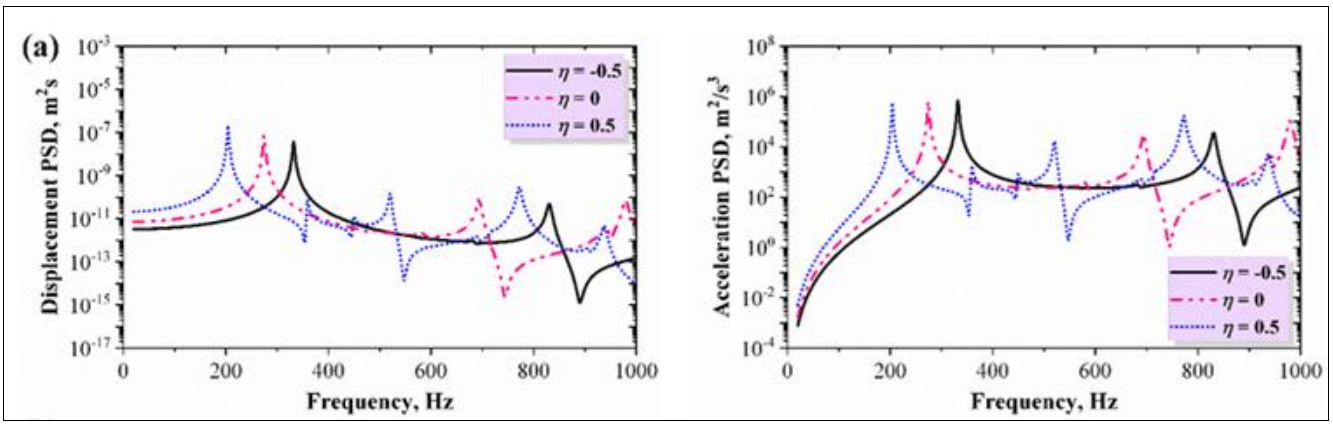

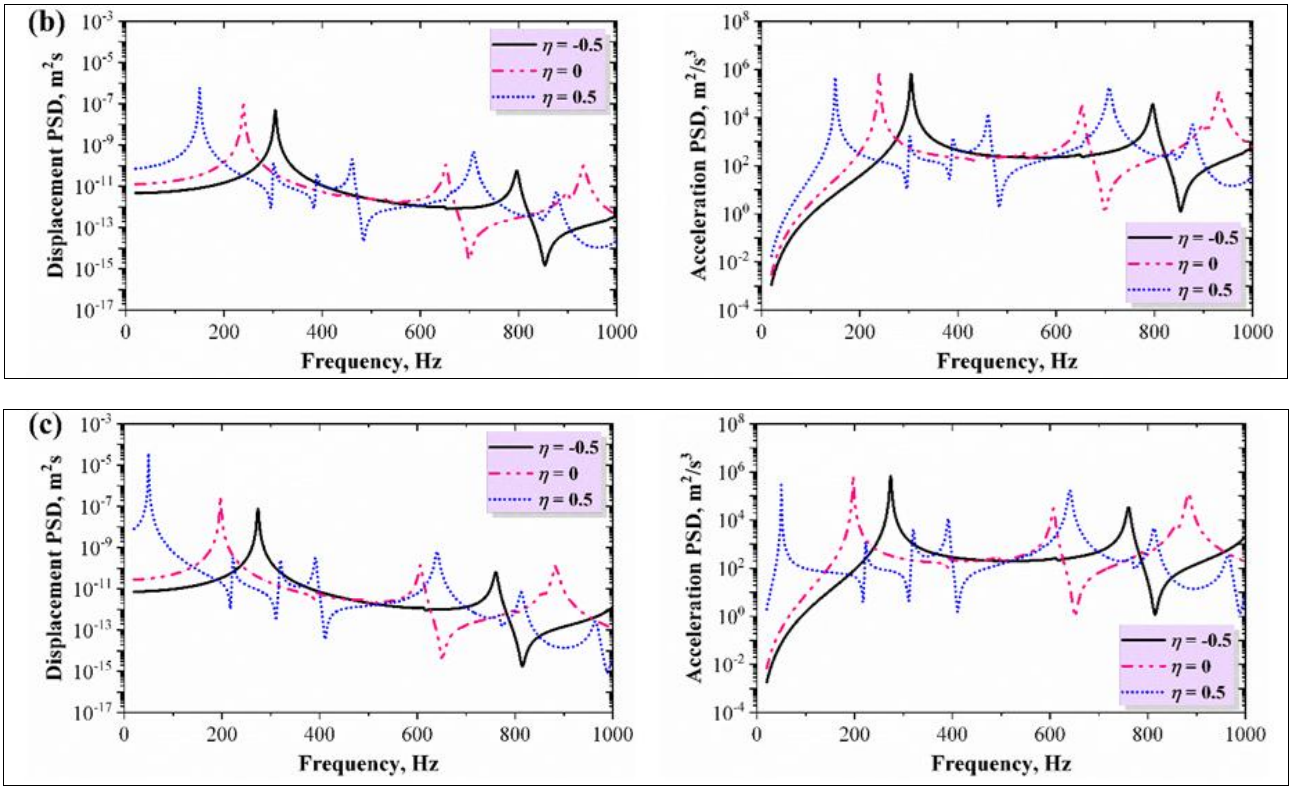

Fig 11: Displacement and acceleration response PSD curves of heated composite laminated plate with different thickness gradients subjected to stationary random excitation; (a) ΔT=0 (b) ΔT=100K (c) ΔT=200K.

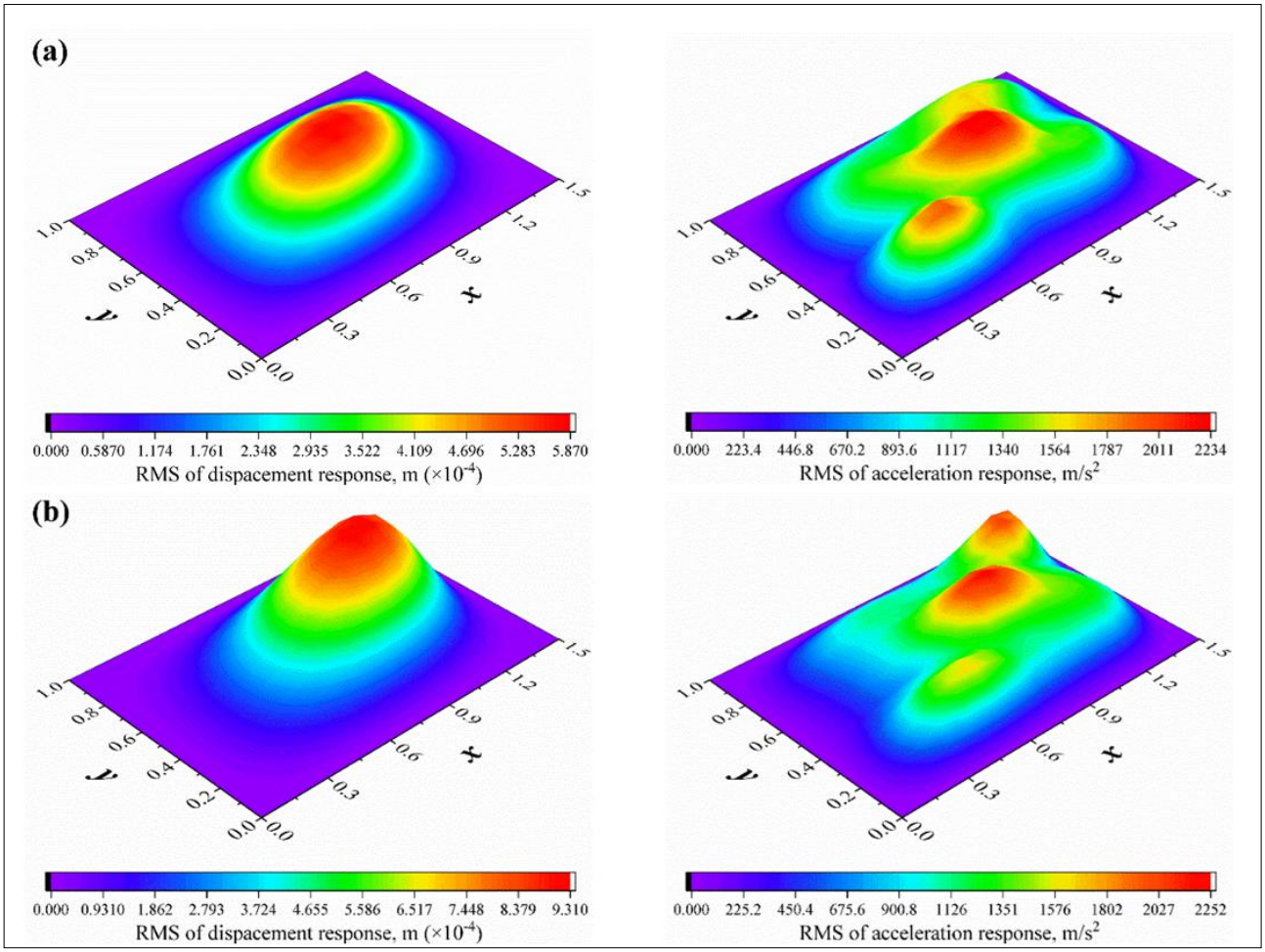

Fig 12: RMS responses of composite laminated plate with different thickness gradients subjected to stationary random excitation; (a) η=0 (b) η=0.5.

Finally, the effect of fiber direction coefficient on the displacement and acceleration response PSD curves of the simply supported plate excited by the band-limited base acceleration is investigated in Fig. 13. The thickness parameters are as η=-0.5, p=1, and other parameters are the same as in previous example. Obviously, the peaks of the PSD curves move to higher frequency range with increasing the fiber gradient coefficient. The amplitude of the first pick of the displacement response curves increases with increasing the temperature difference and decreasing the fiber gradient coefficient. The displacement and acceleration RMS responses of the composite laminated plate with different fiber direction coefficients are shown in Fig. 14. It can be found from that the maximum values of RMS responses of the plate with linear fiber (λ=0) are greater than those of curvilinear fiber.

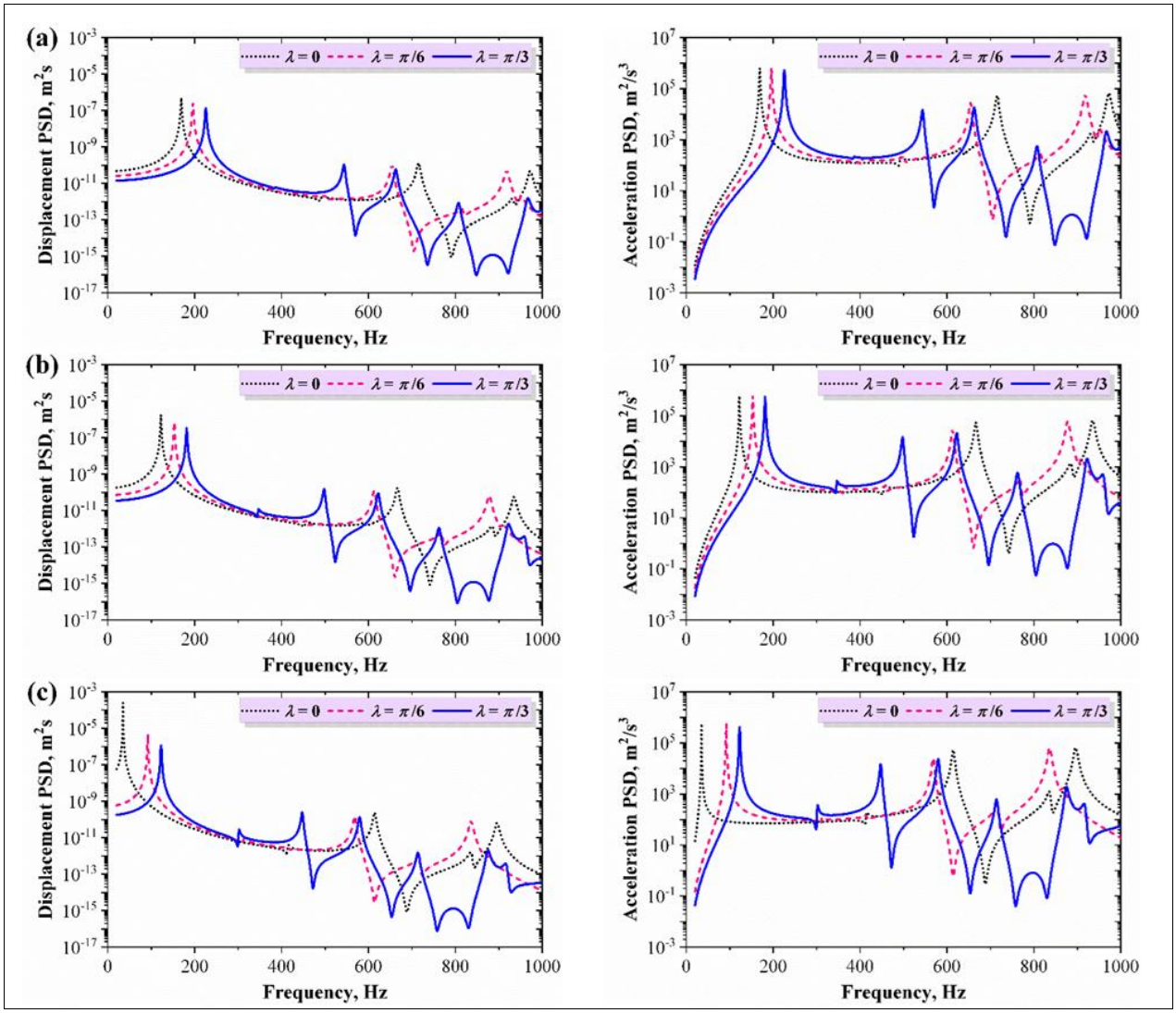

Fig 13: Displacement and acceleration response PSD curves of heated composite laminated plate with different fiber direction coefficients subjected to stationary random excitation; (a) ΔT=0 (b) ΔT=100K (c) ΔT=200K.

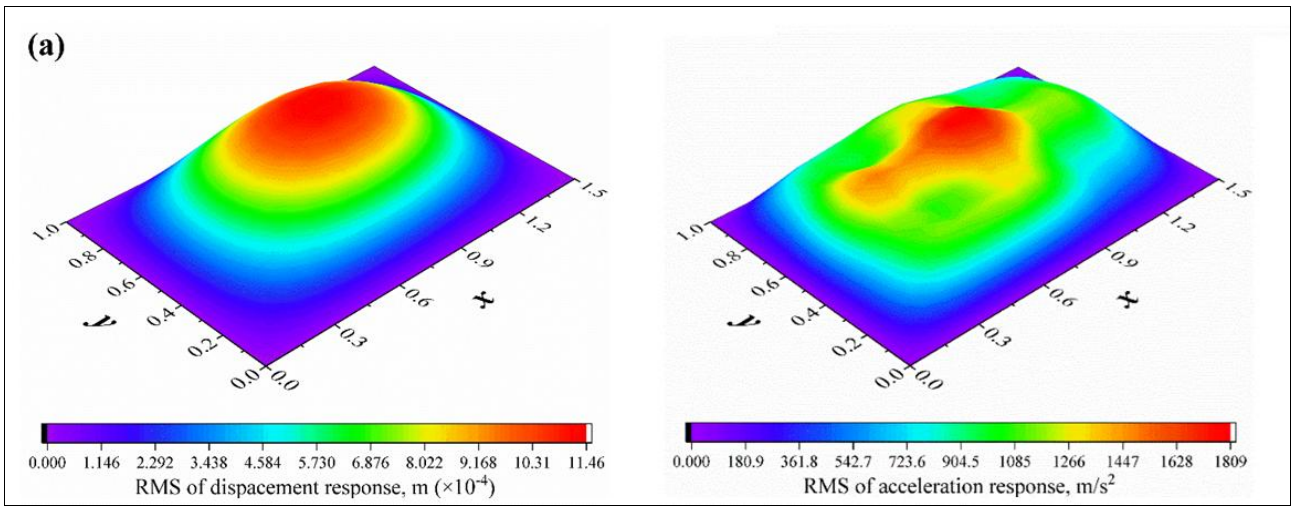

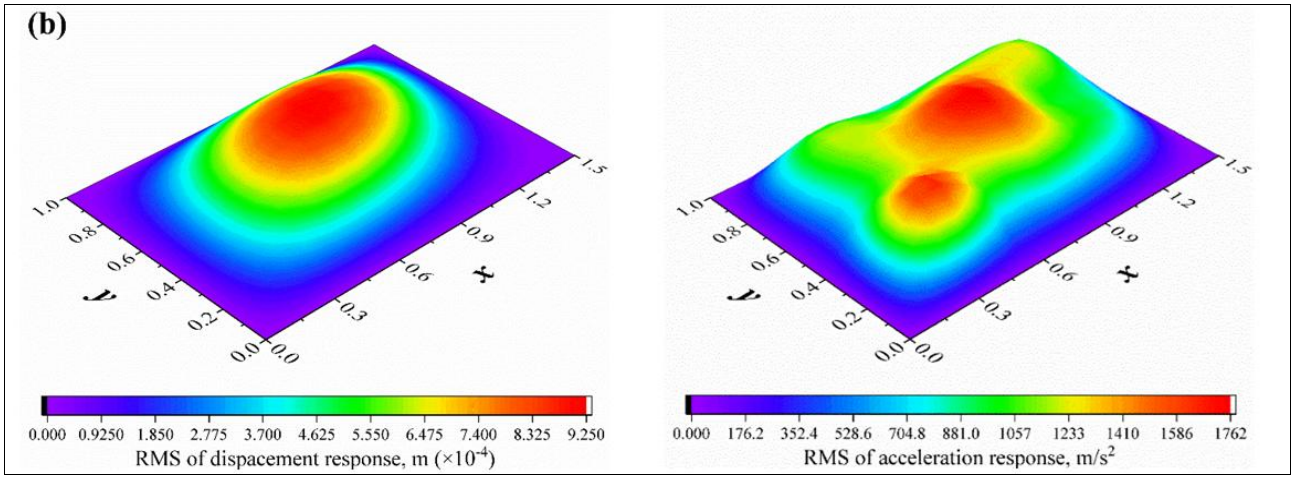

Fig 14: RMS responses of composite laminated plate with different fiber direction coefficients subjected to stationary random excitation; (a) λ=0 (b) λ=π/6.

Conclusions

This paper presents MJPI method for the free vibration and stationary stochastic response analyses of heated composite laminated plate with varying thickness and curvilinear fiber. The Hamilton's principle and FSDT are employed to establish the governing equations of heated composite laminated plate with varying thickness and curvilinear fiber. The stiffness coefficients for varying thickness and curvilinear fiber are derived, and the thermal strains induced by the temperature difference are expressed by using the nonlinear part of the Green-Lagrange strain. The displacement components of the plate are approximated by the proposed MJPI shape function. The boundary conditions are achieved by the three linear springs and two rotational springs distributed alone the bounds of the plate structure. The accuracy and reliability of the proposed method are verified through the convergence study and the comparisons of present results with those from available literature and finite element software. Several numerical examples are provided to illustrate the free vibration and stationary stochastic response behaviors of the composite laminated plate with different parameters such as temperature difference, fiber direction coefficient, thickness gradient and thickness power index.

Acknowledgment

I would like to take the opportunity to express my hearted gratitude to all those who make a contribution to the completion of my article.

Conflict of interest

The authors declare that there is no conflict of interest regarding the publication of this paper.

References

1. Kaveh A, Dadras A, Geran Malek N. Robust design optimization of laminated plates under uncertain bounded buckling loads. Structural and Multidisciplinary Optimization. 2019;59(3):877-891.
2. Shi D, Liu T, Wang Q, Lan Q. Vibration analysis of arbitrary straight-sided quadrilateral plates using a simple first-order shear deformation theory. Results in Physics. 2018;11:201-211.
3. Sayyad AS, Ghugal YM. Static and free vibration analysis of doubly curved functionally graded material shells. Composite Structures. 2021;269:114045.
4. Zhang C, Jin G, Ma X, Ye T. Vibration analysis of circular cylindrical double-shell structures under general coupling and end boundary conditions. Applied Acoustics. 2016;110:176-193.
5. Qin B, Zhong R, Wu Q, Wang T, Wang Q. A unified formulation for free vibration of laminated plate through Jacobi-Ritz method. Thin-Walled Structures. 2019;144:106354.
6. Zhang H, Shi D, Wang Q. An improved Fourier series solution for free vibration analysis of moderately thick laminated composite rectangular plates with non-uniform boundary conditions. International Journal of Mechanical Sciences. 2017;121:1-20.
7. Wang Q, Xie F, Qin B, Zhong R, Yu H. Dynamics and power flow control of irregular elastic coupled plate systems: Precise modeling and experimental validation. International Journal of Mechanical Sciences. 2020;185:105760.
8. Zhao J, Wang Q, Deng X, Choe K, Zhong R, Shuai C. Free vibrations of functionally graded porous rectangular plates with uniform elastic boundary conditions. Composites Part B. 2019;168:106-120.
9. Javani M, Kiani Y, Eslami MR. Application of generalized differential quadrature element method to free vibration of FG-GPLRC T-shaped plates. Engineering Structures. 2021;242:112510.
10. Liu T, Hu G, Wang A, Wang Q. A unified formulation for free in-plane vibrations of arbitrarily shaped straight-sided quadrilateral and triangular thin plates. Applied Acoustics. 2019;155:407-422.
11. Zhang H, Zhu R, Shi D, Wang Q. A simplified plate theory for vibration analysis of composite laminated sector, annular and circular plates. Thin-Walled Structures. 2019;143:106252.
12. Pang F, Li H, Chen H, Shan Y. Free vibration analysis of combined composite laminated cylindrical and spherical shells

with arbitrary boundary conditions. Mechanics of Advanced Materials and Structures. 2021;28:182-199.
13. Amabili M. Non-linearities in rotation and thickness deformation in a new third-order thickness deformation theory for static and dynamic analysis of isotropic and laminated doubly curved shells. International Journal of Non-Linear Mechanics. 2015;69:109-128.
14. Jin G, Yang C, Liu Z. Vibration and damping analysis of sandwich viscoelastic-core beams using Reddy's higher-order theory. Composite Structures. 2016;140:390-409.
15. Mohammadi M, Mohseni E, Moeinfar M. Bending, buckling and free vibration analysis of incompressible functionally graded plates using higher-order shear and normal deformable plate theory. Applied Mathematical Modelling. 2019;69:47-62.
16. Qu Y, Wu S, Li H, Meng G. Three-dimensional free and transient vibration analysis of composite laminated and sandwich rectangular parallelepipeds: Beams, plates and solids. Composites Part B. 2015;73:96-110.
17. Ye T, Jin G, Su Z. Three-dimensional vibration analysis of functionally graded sandwich deep open spherical and cylindrical shells with general restraints. Journal of Vibration and Control. 2016;22(15):3326-3354.
18. Kwak SH, Kim KH, Pyon SB, Ri YH, Ri CG. A new meshfree approach for three-dimensional free vibration analysis of thick laminated doubly curved shells of revolution. Engineering Analysis with Boundary Elements. 2022;134:199-218.
19. Jin G, Ye T, Su Z. Structural Vibration: A Uniform Accurate Solution for Laminated Beams, Plates and Shells with General Boundary Conditions. Springer; 2015.
20. Jin G, Shi S, Su Z, Li S, Liu Z. A modified Fourier-Ritz approach for free vibration analysis of laminated functionally graded shallow shells with general boundary conditions. International Journal of Mechanical Sciences. 2015;93:256-269.
21. Ye T, Jin G, Su Z, Chen Y. A modified Fourier solution for vibration analysis of moderately thick laminated plates with general boundary restraints and internal line supports. International Journal of Mechanical Sciences. 2014;80:29-46.
22. Li H, Pang F, Li Y, Gao C. Application of first-order shear deformation theory for vibration analysis of functionally graded doubly curved shells of revolution. Composite Structures. 2019;212:22-42.
23. Jooybar N, Malekzadeh P, Fiouz A, Vaghefi M. Thermal effect on free vibration of functionally graded truncated conical shell panels. Thin-Walled Structures. 2016;103:45-61.
24. Shakouri M. Free vibration analysis of functionally graded rotating conical shells in thermal environment. Composites Part B. 2019;163:574-584.
25. Yadav A, Amabili M, Panda SK, Dey T. Non-linear vibration response of functionally graded circular cylindrical shells subjected to thermo-mechanical loading. Composite Structures. 2019;229:111430.
26. Liu T, Zhang W, Mao JJ, Zheng Y. Nonlinear breathing vibrations of eccentric rotating composite laminated circular cylindrical shells subjected to temperature, rotating speed and external excitations. Mechanical Systems and Signal Processing. 2019;127:463-498.
27. Duc ND, Quan TQ, Khoa ND. Nonlinear dynamic response and vibration of imperfect functionally graded carbon nanotube reinforced composite double-curved shallow shells subjected to blast load and temperature. Aerospace Science and Technology. 2017;71:360-372.
28. Esfarjani SM, Salehi M, Ghassemi A. Effect of multiple damages and temperature changes on the natural frequency. Journal of Theoretical and Applied Mechanics. 2017;55:813-822.
29. Soureshjani AH, Talebitooti R, Talebitooti M. Thermal effects on the free vibration of joined FG-CNTRC conical-conical shells. Thin-Walled Structures. 2020;156:106960.
30. Kumar P, Harsha SP. Vibration response analysis of exponential functionally graded piezoelectric plates subjected to thermo-electro-mechanical load. Composite Structures. 2021;267:113901.
31. Kumar A, Kumar D. Vibration analysis of functionally graded stiffened shallow shells under thermo-mechanical loading. Materials Today: Proceedings. 2021;44:4590-4595.
32. Routa M, Hota SS, Karmakar A. Thermoelastic free vibration response of graphene-reinforced laminated composite shells. Engineering Structures. 2019;178:179-190.
33. Tornabene F, Viscoti M, Dimitri R, Reddy JN. Higher-order theories for vibration study of doubly curved anisotropic shells with variable thickness and isogeometric mapped geometry. Composite Structures. 2021;267:113829.
34. Kwak SH, Kim KH, Jon SJ, Yun JG, Pak CI. Free vibration analysis of laminated rectangular plates with varying thickness using Legendre-radial point interpolation method. Computers and Mathematics with Applications. 2022;117:187-205.
35. Li H, Pang F, Miao X, Li Y. Jacobi-Ritz method for free vibration analysis of uniform and stepped circular cylindrical shells with arbitrary boundary conditions: A unified formulation. Computers and Mathematics with Applications. 2019;77:427-440.
36. Taati E, Fallah F, Ahmadian MT. Closed-form solution for free vibration of variable-thickness cylindrical shells rotating with a constant angular velocity. Thin-Walled Structures. 2021;166:108062.
37. Quoc TH, Huan DT, Phuong HT. Vibration characteristics of rotating functionally graded circular cylindrical shells with variable thickness under thermal environment. International Journal of Pressure Vessels and Piping. 2021;193:104452.
38. Nie G, Hu H, Zhong Z, Chen X. A complex Fourier series solution for free vibration of arbitrary straight-sided quadrilateral laminates with variable angle tows. Mechanics of Advanced Materials and Structures. 2020;doi:10.1080/15376494.2020.1807660.
39. Kwak SH, Kim KH, Kim J, Kim YC, Kim Y, Pang KJ. Meshfree approach for free vibration analysis of laminated sectorial and rectangular plates with varying fiber angle. Thin-Walled Structures. 2022;174:109070.
40. Haji Hosseinloo A, Yap FF. Analytical random vibration analysis of boundary-excited thin rectangular plates. International Journal of Structural Stability and Dynamics. 2013;13:1250062.

41. Gao W, Chen J, Cui M, Cheng Y. Dynamic response analysis of linear stochastic truss structures under stationary random excitation. Journal of Sound and Vibration. 2005;281:311-321.
42. Dogan V. Nonlinear vibration of functionally graded plates under random excitation. Composite Structures. 2013;95:366-374.
43. Zhou K, Ni Z, Huang X, Hua H. Stationary and non-stationary stochastic response analysis of composite laminated plates with aerodynamic and thermal loads. International Journal of Mechanical Sciences. 2020;173:105461.
44. Chen G, Zhou J, Yang D. Benchmark solutions of stationary random vibration for rectangular thin plates based on discrete analytical method. Probabilistic Engineering Mechanics. 2017;50:17-24.
45. Yang D, Chen G, Zhou J. Exact solutions of fully non-stationary random vibration for rectangular Kirchhoff plates using discrete analytical method. International Journal of Structural Stability and Dynamics. 2017;17:1750126.

Appendix A: Components of matrix *k*

$$A_{ij}^{pq}=\sum_{k=1}^{N_L}\int_{z_k}^{z_{k+1}}Q_{ij}^{k}\alpha_{pq}^{k}dz,\ B_{ij}^{pq}=\sum_{k=1}^{N_L}\int_{z_k}^{z_{k+1}}Q_{ij}^{k}\alpha_{pq}^{k}zdz,\ D_{ij}^{pq}=\sum_{k=1}^{N_L}\int_{z_k}^{z_{k+1}}Q_{ij}^{k}\alpha_{pq}^{k}z^2dz$$

$$\left[A_{ij,x}\quad B_{ij,x}\quad D_{ij,x}\right]=\frac{\partial}{\partial x}\left[A_{ij}\quad B_{ij}\quad D_{ij}\right],\ \left[A_{ij,x}^{pq}\quad B_{ij,x}^{pq}\quad D_{ij,x}^{pq}\right]=\frac{\partial}{\partial x}\left[A_{ij}^{pq}\quad B_{ij}^{pq}\quad D_{ij}^{pq}\right]$$

$$\begin{aligned}k_{11}=&\left[A_{11}-\Delta T\left(A_{11}^{11}+A_{12}^{22}+A_{16}^{12}\right)\right]\frac{\partial^2}{\partial x^2}+\left[A_{66}-\Delta T\left(A_{12}^{11}+A_{22}^{22}+A_{26}^{12}\right)\right]\frac{\partial^2}{\partial y^2}\\&+2\left[A_{16}-\Delta T\left(A_{16}^{11}+A_{26}^{22}+A_{66}^{12}\right)\right]\frac{\partial^2}{\partial x\partial y}+\left[A_{11,x}-\Delta T\left(A_{11,x}^{11}+A_{12,x}^{22}+A_{16,x}^{12}\right)\right]\frac{\partial}{\partial x}\\&+\left[A_{16,x}-\Delta T\left(A_{16,x}^{11}+A_{26,x}^{22}+A_{66,x}^{12}\right)\right]\frac{\partial}{\partial y}\end{aligned}$$

$$k_{12}=A_{16}\frac{\partial^2}{\partial x^2}+A_{26}\frac{\partial^2}{\partial y^2}+(A_{12}+A_{66})\frac{\partial^2}{\partial x\partial y}+A_{16,x}\frac{\partial}{\partial x}+A_{12,x}\frac{\partial}{\partial y}$$

$$k_{15}=B_{16}\frac{\partial^2}{\partial x^2}+B_{26}\frac{\partial^2}{\partial y^2}+(B_{12}+B_{66})\frac{\partial^2}{\partial x\partial y}+B_{16,x}\frac{\partial}{\partial x}+B_{12,x}\frac{\partial}{\partial y}$$

$$k_{21}=A_{16}\frac{\partial^2}{\partial x^2}+A_{26}\frac{\partial^2}{\partial y^2}+(A_{12}+A_{66})\frac{\partial^2}{\partial x\partial y}+A_{16,x}\frac{\partial}{\partial x}+A_{66,x}\frac{\partial}{\partial y}$$

$$k_{24}=B_{16}\frac{\partial^2}{\partial x^2}+B_{26}\frac{\partial^2}{\partial y^2}+(B_{12}+B_{66})\frac{\partial^2}{\partial x\partial y}+B_{16,x}\frac{\partial}{\partial x}+B_{66,x}\frac{\partial}{\partial y}$$

$$\begin{aligned}k_{25}=k_{52}=&\left[B_{66}-\Delta T\left(B_{11}^{11}+B_{12}^{22}+B_{16}^{12}\right)\right]\frac{\partial^2}{\partial x^2}+\left[B_{22}-\Delta T\left(B_{12}^{11}+B_{22}^{22}+B_{26}^{12}\right)\right]\frac{\partial^2}{\partial y^2}\\&+2\left[B_{26}-\Delta T\left(B_{16}^{11}+B_{26}^{22}+B_{66}^{12}\right)\right]\frac{\partial^2}{\partial x\partial y}+\left[B_{66,x}-\Delta T\left(B_{11,x}^{11}+B_{12,x}^{22}+B_{16,x}^{12}\right)\right]\frac{\partial}{\partial x}\\&+\left[B_{26,x}-\Delta T\left(B_{16,x}^{11}+B_{26,x}^{22}+B_{66,x}^{12}\right)\right]\frac{\partial}{\partial y}\end{aligned}$$

$$k_{34}=A_{55}\frac{\partial}{\partial x}+A_{45}\frac{\partial}{\partial y}+A_{55,x}$$

$$k_{35}=A_{45}\frac{\partial}{\partial x}+A_{44}\frac{\partial}{\partial y}+A_{45,x}$$

$$k_{42}=B_{16}\frac{\partial^2}{\partial x^2}+B_{26}\frac{\partial^2}{\partial y^2}+(B_{12}+B_{66})\frac{\partial^2}{\partial x\partial y}+B_{16,x}\frac{\partial}{\partial x}+B_{12,x}\frac{\partial}{\partial y}$$

$$k_{43} = -A_{55}\frac{\partial}{\partial x} - A_{45}\frac{\partial}{\partial y}$$

$$k_{45} = D_{16}\frac{\partial^2}{\partial x^2} + D_{26}\frac{\partial^2}{\partial y^2} + (D_{12} + D_{66})\frac{\partial^2}{\partial x \partial y} + D_{16,x}\frac{\partial}{\partial x} + D_{12,x}\frac{\partial}{\partial y} - A_{45}$$

$$k_{51} = B_{16}\frac{\partial^2}{\partial x^2} + B_{26}\frac{\partial^2}{\partial y^2} + (B_{12} + B_{66})\frac{\partial^2}{\partial x \partial y} + B_{16,x}\frac{\partial}{\partial x} + B_{66,x}\frac{\partial}{\partial y}$$

$$k_{53} = -A_{45}\frac{\partial}{\partial x} - A_{44}\frac{\partial}{\partial y}$$

$$\begin{aligned} k_{55} = &\left[D_{66} - \Delta T\left(D_{11}^{11} + D_{12}^{22} + D_{16}^{12}\right)\right]\frac{\partial^2}{\partial x^2} + \left[D_{22} - \Delta T\left(D_{12}^{11} + D_{22}^{22} + D_{26}^{12}\right)\right]\frac{\partial^2}{\partial y^2} \\ &+ 2\left[D_{26} - \Delta T\left(D_{16}^{11} + D_{26}^{22} + D_{66}^{12}\right)\right]\frac{\partial^2}{\partial x \partial y} + \left[D_{66,x} - \Delta T\left(D_{11,x}^{11} + D_{12,x}^{22} + D_{16,x}^{12}\right)\right]\frac{\partial}{\partial x} \\ &+ \left[D_{26,x} - \Delta T\left(D_{16,x}^{11} + D_{26,x}^{22} + D_{66,x}^{12}\right)\right]\frac{\partial}{\partial y} - A_{44} \end{aligned}$$

Appendix B: Components of matrix c_x

$$c_{x11} = \left[A_{11} - \Delta T\left(A_{11}^{11} + A_{12}^{22} + A_{16}^{12}\right)\right]\frac{\partial}{\partial x} + \left[A_{16} - \Delta T\left(A_{16}^{11} + A_{26}^{22} + A_{66}^{12}\right)\right]\frac{\partial}{\partial y}$$

$$c_{x12} = A_{16}\frac{\partial}{\partial x} + A_{12}\frac{\partial}{\partial y}$$

$$c_{x13} = c_{x23} = c_{x31} = c_{x32} = c_{x43} = c_{x53} = 0$$

$$c_{x14} = \left[B_{11} - \Delta T\left(B_{11}^{11} + B_{12}^{22} + B_{16}^{12}\right)\right]\frac{\partial}{\partial x} + \left[B_{16} - \Delta T\left(B_{16}^{11} + B_{26}^{22} + B_{66}^{12}\right)\right]\frac{\partial}{\partial y}$$

$$c_{x15} = B_{16}\frac{\partial}{\partial x} + B_{12}\frac{\partial}{\partial y}$$

$$c_{x21} = A_{16}\frac{\partial}{\partial x} + A_{66}\frac{\partial}{\partial y}$$

$$c_{x22} = \left[A_{66} - \Delta T\left(A_{11}^{11} + A_{12}^{22} + A_{16}^{12}\right)\right]\frac{\partial}{\partial x} + \left[A_{26} - \Delta T\left(A_{16}^{11} + A_{26}^{22} + A_{66}^{12}\right)\right]\frac{\partial}{\partial y}$$

$$c_{x24} = B_{16}\frac{\partial}{\partial x} + B_{66}\frac{\partial}{\partial y}$$

$$c_{x33} = \left[A_{55} - \Delta T\left(A_{11}^{11} + A_{12}^{22} + A_{16}^{12}\right)\right]\frac{\partial}{\partial x} + \left[A_{45} - \Delta T\left(A_{16}^{11} + A_{26}^{22} + A_{66}^{12}\right)\right]\frac{\partial}{\partial y}$$

$$c_{x34} = A_{55}$$

$$c_{x35} = A_{45}$$

$$c_{x42} = B_{16}\frac{\partial}{\partial x} + B_{12}\frac{\partial}{\partial y}$$

$$c_{x45} = D_{16}\frac{\partial}{\partial x} + D_{12}\frac{\partial}{\partial y}$$

$$c_{x51} = B_{16}\frac{\partial}{\partial x} + B_{66}\frac{\partial}{\partial y}$$

$$c_{x54} = D_{16}\frac{\partial}{\partial x} + D_{66}\frac{\partial}{\partial y}$$

$$c_{x55} = \left[D_{66} - \Delta T\left(D_{11}^{11} + D_{12}^{22} + D_{16}^{12} \right) \right]\frac{\partial}{\partial x} + \left[D_{26} - \Delta T\left(D_{16}^{11} + D_{26}^{22} + D_{66}^{12} \right) \right]\frac{\partial}{\partial y}$$

Appendix C: Components of matrix c_y

$$c_{y11} = \left[A_{16} - \Delta T\left(A_{16}^{11} + A_{26}^{22} + A_{66}^{12} \right) \right]\frac{\partial}{\partial x} + \left[A_{66} - \Delta T\left(A_{12}^{11} + A_{22}^{22} + A_{26}^{12} \right) \right]\frac{\partial}{\partial y}$$

$$c_{y12} = A_{66}\frac{\partial}{\partial x} + A_{26}\frac{\partial}{\partial y}$$

$$c_{y13} = c_{y23} = c_{y31} = c_{y32} = c_{y43} = c_{y53} = 0$$

$$c_{y15} = B_{66}\frac{\partial}{\partial x} + B_{26}\frac{\partial}{\partial y}$$

$$c_{y21} = A_{12}\frac{\partial}{\partial x} + A_{26}\frac{\partial}{\partial y}$$

$$c_{y24} = B_{12}\frac{\partial}{\partial x} + B_{26}\frac{\partial}{\partial y}$$

$$c_{y34} = A_{45}$$

$$c_{y35} = A_{44}$$

$$c_{y41} = \left[B_{16} - \Delta T\left(B_{16}^{11} + B_{26}^{22} + B_{66}^{12} \right) \right]\frac{\partial}{\partial x} + \left[B_{66} - \Delta T\left(B_{12}^{11} + B_{22}^{22} + B_{26}^{12} \right) \right]\frac{\partial}{\partial y}$$

$$c_{y42} = B_{66}\frac{\partial}{\partial x} + B_{26}\frac{\partial}{\partial y}$$

$$c_{y44} = \left[D_{16} - \Delta T\left(D_{16}^{11} + D_{26}^{22} + D_{66}^{12} \right) \right]\frac{\partial}{\partial x} + \left[D_{66} - \Delta T\left(D_{12}^{11} + D_{22}^{22} + D_{26}^{12} \right) \right]\frac{\partial}{\partial y}$$

$$c_{y51} = B_{12}\frac{\partial}{\partial x} + B_{26}\frac{\partial}{\partial y}$$

$$c_{y54} = D_{12}\frac{\partial}{\partial x} + D_{26}\frac{\partial}{\partial y}$$

$$c_{y55} = \left[D_{26} - \Delta T\left(D_{16}^{11} + D_{26}^{22} + D_{66}^{12} \right) \right]\frac{\partial}{\partial x} + \left[D_{22} - \Delta T\left(D_{12}^{11} + D_{22}^{22} + D_{26}^{12} \right) \right]\frac{\partial}{\partial y}$$